PION-NUCLEON SCATTERING AND CHARGE SYMMETRY

Thesis for the Degree of M. S.
MICHIGAN STATE UNIVERSITY

Justin Huang

1959

PION - NUCLEON SCATTERING AND CHARGE SYMMETRY

By

Justin Huang

A THESIS

Submitted to the College of Science and Arts
Michigan State University of Agriculture and
Applied Science in partial fulfillment of
the requirements for the degree of

MASTER OF SCIENCE

Department of Physics

1959

ACKNOWLEDGEMENT

I am most grateful to Dr. J. Ballam for sponsoring and suggesting the problem. His continued help and guidance is greatly appreciated. I am also deeply indebted to John Scandrett for much help on the problem. Thanks to Dr. W. Walker, Dr. J. Kovacs, and Dr. D. Lichtenberg for checking parts of the manuscript and making helpful suggestions. The help of Mrs. E. James in scanning and preparing the graphs and David Balzarini in scanning is also greatly appreciated.

PION - NUCLEON SCATTERING AND CHARGE SYMMETRY

By

Justin Huang

AN ABSTRACT

Submitted to the College of Science and Arts
Michigan State University of Agriculture and
Applied Science in partial fulfillment of
the requirements for the degree of

MASTER OF SCIENCE
Department of Physics
1959

Approved Joseph Bellam 2/26/59

ABSTRACT

An analysis of negative pion - neutron scattering at 460 mev in a propane bubble chamber has been made in order to verify the hypothesis of charge symmetry in pion - nucleon interactions. A comparison of the angular distribution in (π^-,n) and (π^+,p) scattering at equivalent energies was made for this purpose. Since the (π^+,p) data were obtained in hydrogen, corrections for nucleon motion, assuming a Fermi sphere of 191 mev/c, as well as for diffraction from the carbon nucleus, using a black sphere model, were carried out. Applying a χ^2 test, the resulting (π^-,n) angular distribution fits a least squares fit of the (π^+,p) data with a probability of 0.054 for the entire curve and a probability of 0.20 for the part of the curve corresponding to laboratory angles greater than 33 degrees.

TABLE OF CONTENTS

I INTRODUCTION

An important particle in the mystery of nuclear physics is the pi meson. According to Yukawa"s theory, the pi meson plays the same role in a nuclear field as the photon plays in the electromagnetic field.[1] With the discovery of the artificially produced pi meson; its mass, spin, lifetime for weak decay and parity became well established. The interaction of the pi meson with nucleons is, however, not so well established. One method of studying the interaction is to observe the scattering of pi mesons from nucleons. An experiment to measure pi meson proton scattering is relatively simple to perform since there are sources of free protons available. However, it is very difficult to study pi meson neutron scattering, since there are no stationary free neutrons available in nature. All stable sources of neutrons are found in a bound state (inside a nucleus). However, from the principle of charge symmetry, we can predict the interaction of a pi meson with neutrons by studying the interaction of a pi meson with protons.

To explain charge symmetry, it is convenient to introduce the idea of isotopic spin.[2] Isotopic spin formalism makes use of the similarities between a proton and a neutron. They have the same spin and mass, but a

different charge. Apart from electromagnetic effects, they behave the same way in nuclear matter. They could be thought of as just one particle (a nucleon) in two different charge states. We introduce a new quantum number "M_t" and give it a value of +1/2 for a proton and -1/2 for a neutron. The state of a nucleon is now also determined by this new quantum number. The Pauli exclusion principle can now be generalized to exclude the states of any two nucleons with all quantum numbers equal, including M_t. The terminology "spin" was introduced because of the analogous role that the charge states play to the role of ordinary spin in atomic physics, if we neglect spin-orbit interaction. Again in analogy to ordinary spin, we could think of a three dimensional "isotopic spin space", having the three operators:

$$T_x = \begin{pmatrix} 0 & 1 \\ 1 & 0 \end{pmatrix}$$
$$T_y = \begin{pmatrix} 0 & -i \\ i & 0 \end{pmatrix}$$
$$T_z = \begin{pmatrix} 1 & 0 \\ 0 & -1 \end{pmatrix}$$

The quantum number M_t would just be the projection of T on the z axis.

With this knowledge of isotopic spin space, we may now proceed to define charge symmetry. The statement of charge symmetry is that a 180 degree rotation of the isotopic spin vectors about any axis in the xy plane does not change the interaction. The definition

effectively, just changes the sign of M_t. We can now see that from the previous assignment of T_z for a proton and a neutron, (n,n) and (p,p) interactions should be identical. (n,n) equivalent to (p,p) is the definition of charge symmetry that is commonly used. The advantage of the first definition is that it can also be applied to meson - nucleon systems. The pi meson is a charge triplet[3] with T_z = 1,0,-1 corresponding to a π^+, π^0, and π^- respectively. It now follows that by charge symmetry, a proton can be interchanged with a neutron, a π^+ meson can be interchanged with a π^- meson, a π^0 meson can be interchanged with a π^0 meson, and vice versa in any interaction. We can now clearly see that

a. (π^+,p) and (π^-,n)

b. (π^-,p) and (π^+,n)

c. (π^0,p) and (π^0, n)

should be identical interactions.

In this paper, we are interested in an experimental verification of this principle of charge symmetry in pion - nucleon scattering at pion energies of 460 mev. The method used is to compare the angular distributions of negative pions scattered from neutrons and of positive pions scattered from protons in the laboratory system. Previous work similar to this has been performed by J. Ashkin[4] et al. The method used by Ashkin was to compare the total cross sections of positive and negative

pions scattered from deuterium.

Since the protons in this experiment are free and the neutrons are bound in carbon nuclei, both experimentally obtained distributions must be transformed before the comparison can be made. This is described in detail in Section III.

The main proton data were obtained by W. D. Willis[5] who did (π^+,p) scattering at 500 mev using a hydrogen bubble chamber. As will be described in Section III, data from (π^+,p) scattering at 850 mev in a hydrogen chamber by Erwin and Kopp[6] and at 1.1 bev in a propane chamber by Glaser et al[7] will be used in the analysis.

The neutron data were obtained from Walker et al[8] in a propane chamber exposed to 460 mev π^- mesons at the cosmotron.

II EXPERIMENTAL DETAILS

The pion-neutron data was abstracted from 20,000 pictures taken of a propane bubble chamber built by Professor W. D. Walker of the University of Wisconsin which was exposed to a 460 mev negative pion beam at the cosmotron of the Brookhaven National Laboratory. There was no magnetic field. The chamber was photographed by two cameras with their optical axes at right angles to each other. The use of the maximum possible stereo angle allowed for the accurate measurement of the most important quantity in the experiment – the space angles between the various tracks. A sketch of the optical system is shown in figure 1.

In the scanning of the pictures, every event involving an incoming pi meson was recorded. These events were broken down as follows:

Hydrogen

elastic	$\pi^- + p = \pi^- + p$
charge exchange	$\pi^- + p = \pi^o + n$
π^+ production	$\pi^- + p = \pi^+ + \pi^- + n$
π^o production	$\pi^- + p = \pi^o + \pi^- + p$

Carbon

quasi elastic	$\pi^- + p = \pi^- + p$
charge exchange	$\pi^- + p = \pi^o + n$

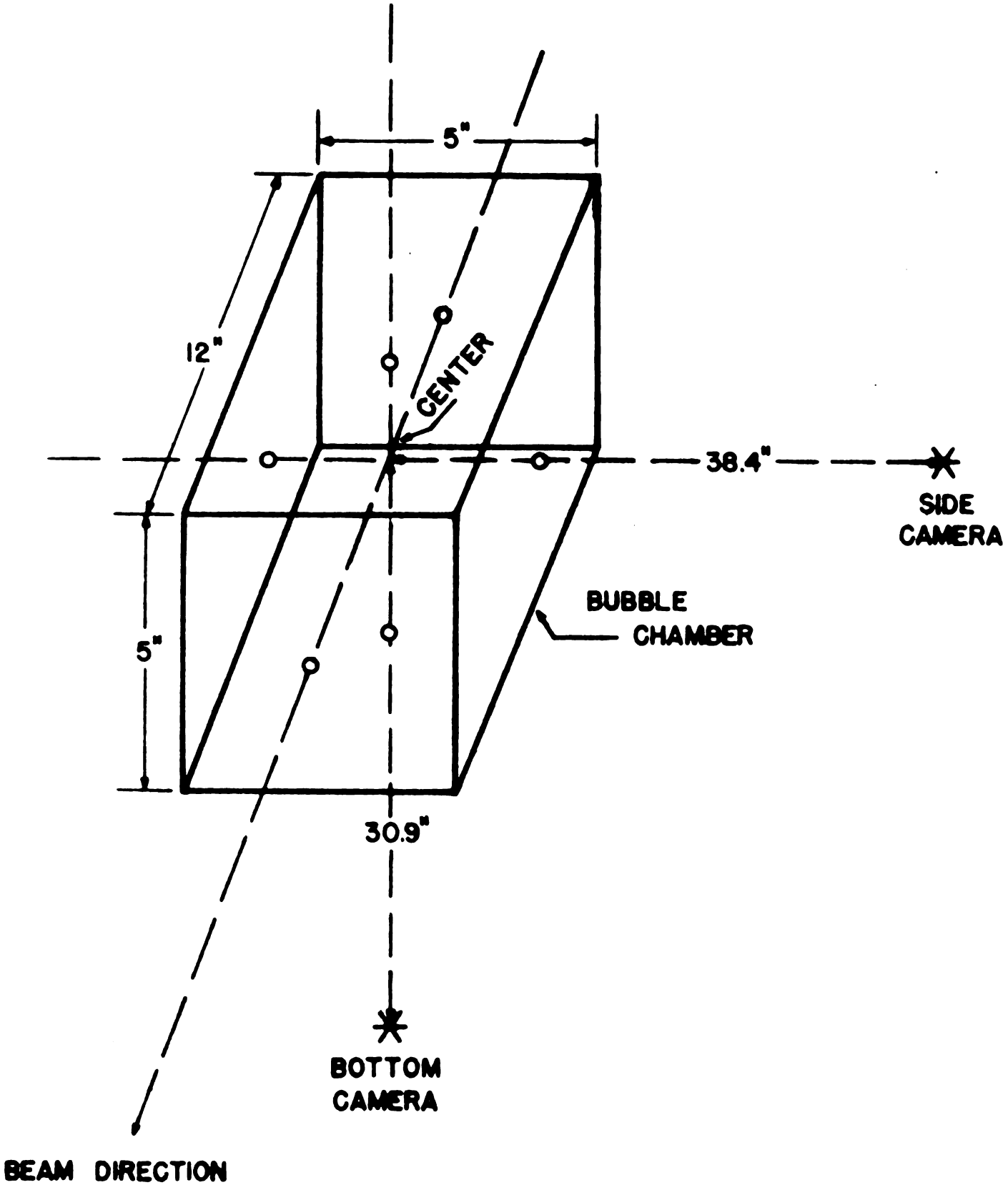
5"
12"
CENTER
38.4"
SIDE
CAMERA
BUBBLE
CHAMBER
5"
30.9"
BOTTOM
CAMERA
BEAM DIRECTION

FIGURE 1

π^+ production	$\pi^- + p = \pi^+ + \pi^- + n$
π^0 production	$\pi^- + p = \pi^0 + \pi^- + p$
deflection	$\pi^- + n = \pi^- + n$
	diffraction off carbon nucleus
π^0 prod. on neutron	$\pi^- + n = \pi^0 + \pi^- + n$
stars	----------

The number of events for each catagory is listed in Table 1.

description	number
elastic	298
quasi elastic	369
π^+ prod. (hydrogen & carbon)	182
π^0 prod. " " "	105
charge exchange " "	464
deflections $> 6^\circ$	905
deflections $< 6^\circ$	219
π^0 prod. on neutron	20
stars with 0 π^-	442
stars with 1 π^-	545
stars with 2 π^-	72
Total	3621

Table 1.

The events of most interest to us were the (π^-,p) elastic scatterings from the hydrogen in the chamber and the (π^-,n) elastic scatterings from the neutrons bound in the carbon of the chamber. In the former case, the kinematics of the event is completely determined from the angles that the scattered pion and the proton make with the initial direction of the incoming pion. An equally good set of variables is the angle of the scattered pion and the range of the proton. The elastic events are separated from the quasi-elastics by a measurement of the coplanarity of the event. With these parameters, one can measure the angle of emission of the scattered pion in the center of mass system. Or from the Lorentz transformation, one has (symbols defined on page 15)

$$(1) \qquad P\cos\theta = \gamma\left(P^*\cos\theta^* + \beta E^*\right)$$

$$(2) \qquad P\sin\theta = P^*\sin\theta^*$$

A set of curves giving θ_π vs θ_p with θ^* and P_π (incoming) as parameters has been plotted so that once the space angles have been measured, the incoming momentum and the corresponding center of mass angle can be quickly determined (See figure 13).

In order to calculate the space angles, the following measurements are made on each elastic scattering (these are all made with respect to a set of fixed axes in the chamber and in each of the two views).

Fig. 2 Deflections.

a. Incoming beam angle.

b. Angle of the scattered pion.

c. Angle of the scattered proton.

d. Co-ordinates of the point of collision.

e. Range of the proton (when available).

f. Tangents of the coplanarity angles, where available.

These data must then be combined to find the space angle. In this process, the two most important corrections are for the conical projection and the index of refraction of the propane (1.25). The details of these calculations are shown in the Appendix. A program for these calculations was made for the digital computer Mistic of the computer laboratory, Michigan State University.

We are concerned in this paper mainly with the deflections. The small angle deflections are considered to be mainly diffraction scatterings from carbon, while the large angle ones are mainly pion-neutron scatterings. A typical deflection is shown in figure 2. It is characterized by a sharp break in a fast pi beam accompanied by no visible recoil tracks. A total of 1090 of these deflections were measured and calculated for their space angles. The following quantities were measured from the conical plane (film).

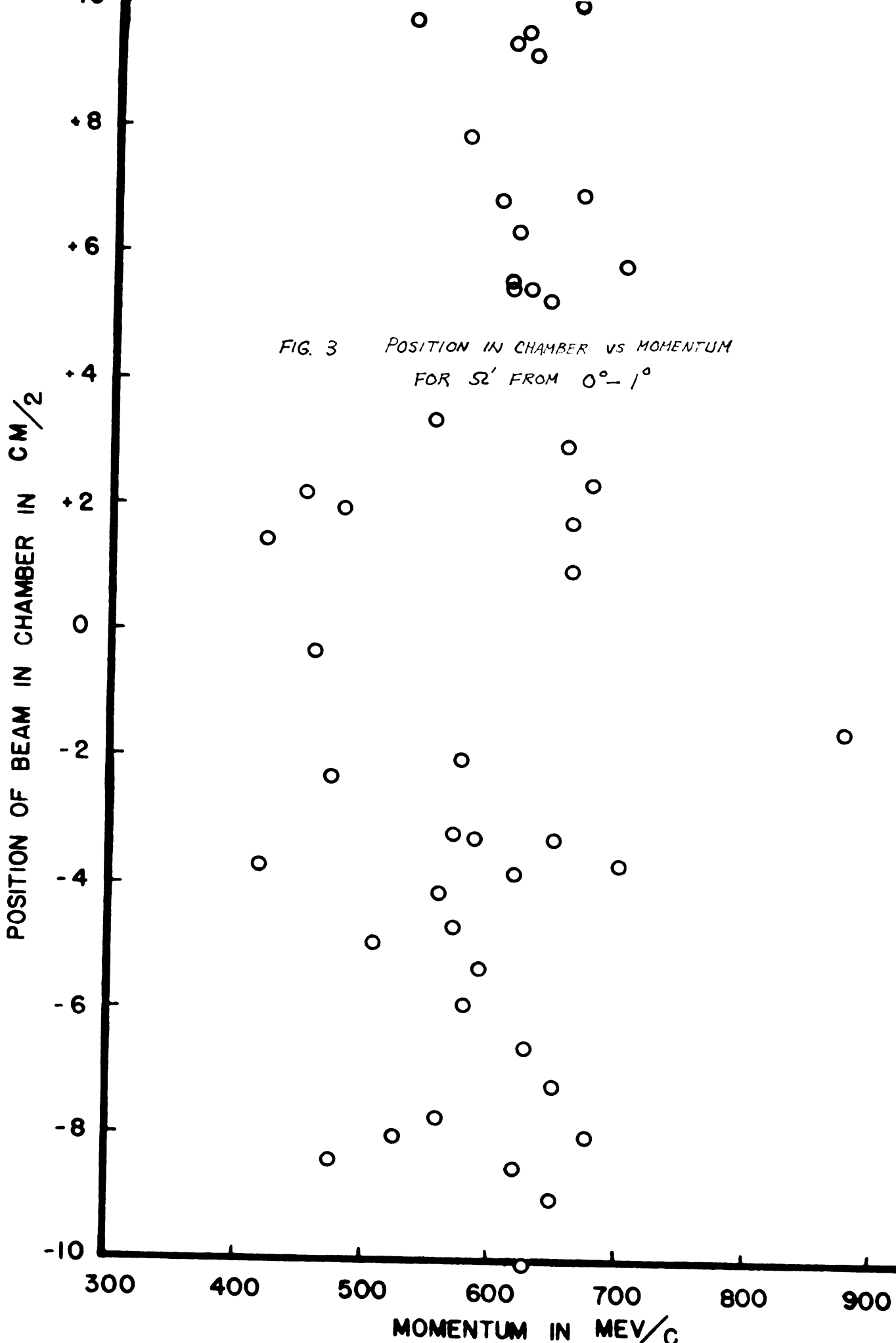

FIG. 3 POSITION IN CHAMBER VS MOMENTUM FOR Ω' FROM $0° - 1°$

Bottom view:

a. beam angle.

b. deflected angle.

c. position of beam in chamber.

Side view:

a. beam angle.

b. deflected angle.

The purpose of the third measurement in the bottom view was to separate the events into different momentum groups. However, a preliminary study made of the sensitivity of the measurement to momentum was negative. About 300 (π^-,p) elastic events were analyzed for the dependence of beam angle and position in chamber to momentum. The momentum of the (π^-,p) elastics were found through other criteria already mentioned. An example of the results is shown in figure 3. The idea of dividing our events into momentum groups was thus quickly abandoned and an average value of 590mev/c was adopted for all incident pions. The space angles were calculated using the analysis scheme derived in the Appendix and by the digital computer Mistic. The approximation that all events occur at the center of the chamber was made to simplify the computations.(an error of at most 1^o in the lab. system).

Using the values $\sigma_T(\pi^-,H)$ = 30 mb and $\sigma_T(\pi^-,C)$ equal to 316 mb determined from experiments by Cool et al;[9,10] the value for σ(deflection) can be determined from

$$(3)\qquad \frac{3\,\sigma(\text{deflection})}{8\,\sigma_T(\pi^-,H)+3\,\sigma_T(\pi^-,C)} = \frac{\text{number of deflections}}{\text{total number of events}}$$

The value for σ(deflection) came out to be 106 mb. The differential cross section $d\sigma/d\Omega$ for deflections can now be calculated using

$$(4)\qquad \frac{d\sigma}{d\Omega} = \frac{\text{no. of intervals}}{4\pi} \times \frac{\text{no. in interval}}{\text{total no. of defl.}} \times \sigma(\text{defl.})$$

The angular distribution $d\sigma/d\Omega$ vs cos θ for all deflections is given in Table 2. The distribution is also illustrated in figures 17 and 18 (the π^- curve). The total cross sections obtained from Cool et al were for anti-coincidence angles up to 6°. This means that all events with angles less than 6° are counted as going straight through. Therefore, in our calculations, we must neglect all deflections with angles less than 6°.

The events classified as deflections have actually a third possible origin besides the two already listed. This other possibility is a $1\pi^-$, 2n star with a fast pi coming off. As a rough check on how many of these events we could have included as deflections, a survey was made in our data for $1\pi^-$, 1p, ?n stars with a fast pi and a backward scattered proton. It is assumed that in these events, a neutron would also have been given off by the carbon nucleus. It is then assumed that the number of $1\pi^-$, 2n stars would not exceed the number of $1\pi^-$, 1p, 1n

stars. The number of $1\pi^-$, 1p, 1n stars found was roughly 28, negligible compared to the total of 1124 deflections found. We shall thus consider the deflections to be just composed of (π^-,n) and diffraction scatterings.

Table 2. Angular Distribution for Deflections.

θ lab. (deg.)	No.	$d\sigma/d\Omega$ mb/str	Error mb/str
6-8	69	308	37
8-10	74	257	30
10-12	84	240	26.2
12-14.1	82	188	20.8
14.1-16.3	80	151	16.9
16.3-18.2	69	130	15.7
18.2-20	47	88.9	13.0
20-23.1	48	45.8	6.6
23.1-25.9	42	40.0	6.2
25.9-28.3	33	31.4	5.5
28.3-32.9	50	23.8	3.4
32.9-36.9	31	14.8	2.7
36.9-45.6	50	9.53	1.34
45.6-66.4	59	3.76	0.49
66.4-90.0	26	1.72	0.34
90.0-120	20	0.76	0.17
120-180	18	0.69	0.16

III CHARGE SYMMETRY

To test the principle of charge symmetry, we will compare the angular distributions related to the (π^+,p) and (π^-,n) scatterings. There are two major difficulties with the (π^-,n) data. As mentioned previously, we can not in general distinguish between a (π^-,n) and a diffraction scattering, especially small angle scatterings. Secondly, the target neutron is bound inside a carbon nucleus; and according to the Fermi gas model, it has a momentum associated with it. We can reduce the second problem by considering a model proposed by Serber[11,12]. In this model, if the target nucleus is small and the incoming momentum is high, we can consider the problem as just the collision of the pion with one nucleon inside the carbon nucleus. The problem is now similar to an ordinary scattering except that the target is in motion.

A. Correction for a Moving Target.

Let us first correct for the moving target. We have a choice of two approaches. One is to smear out the (π^+,p) angular distribution, that is to give the stationary target nucleon various momenta that it would have if it were bound inside a carbon nucleus. A further explanation of this method will be given later. The other approach is to

unsmear the (π^-,n) angular distribution, that is to find out the most likely distribution it would have if the target nucleon were stationary. The former is the much simpler approach and will be adopted here.

The first question that comes to mind is what parameter determines a scattering. In the center of mass coordinate system, this parameter is just the momentum P^* of the particle. However, the (π^-,n) scattering data is available only in the laboratory system. Therefore, we must compare our distribution in the laboratory system. This means that a Lorentz transformation would have to be performed from the center of mass to the laboratory system. In this transformation, another parameter, the velocity of the center of mass "ß" is introduced. Thus, in the laboratory system, our scattering is completely determined by two parameters, P^* and ß.

Let us now look into the actual Fermi momentum of a nucleon inside a nucleus. Several momentum distributions have been proposed which have given reasonable fits to experimental data[13]. One is the Gaussian distribution,

$$(5) \qquad \rho(\bar{P})\, d\bar{P} = \left(\frac{b}{\pi}\right)^{3/2} e^{-bP^2}\, d\bar{P}$$

where the average kinetic energy of a nucleon is 19.3mev which corresponds to a momentum of 191 mev/c. We shall use the Gaussian distribution[17] to adopt the value of

191 mev/c for the momentum of a nucleon inside a nucleus. Assuming that the nucleons are isotropic in direction, the momenta can be represented by a sphere of 191 mev/c where the density of scattering events is uniform over the surface of the sphere. A three dimensional momentum diagram of the initial state of a scattering event is illustrated in figure 4.

The smeared out angular distribution must be the net effect of every possible scattering on the Fermi sphere of 191 mev/c described above. Thus, in smearing out a distribution, we must consider all scatterings on the Fermi sphere. This would involve an integration over the whole surface of the sphere, a messy calculation to perform. To simplify the task, we shall instead slice up the sphere into 32 parts such that each of the 32 dissected parts represents an equal surface area on the original sphere. Taking a representative point on the outside surface of each of the 32 parts, we shall calculate an angular distribution for that point. The net effect of the whole Fermi sphere will then be the average of the 32 angular distributions.

To obtain an angular distribution for a particular point on the sphere, we must remember that the laboratory angular distribution depends only on P^* and β. Available to us are the experimental angular distributions of (π^+,p) scattering with stationary targets at energies of

$\bar{P}_\pi$ - MOMENTUM OF π MESON BEAM

$\bar{P}_N$ - MOMENTUM OF TARGET NUCLEON

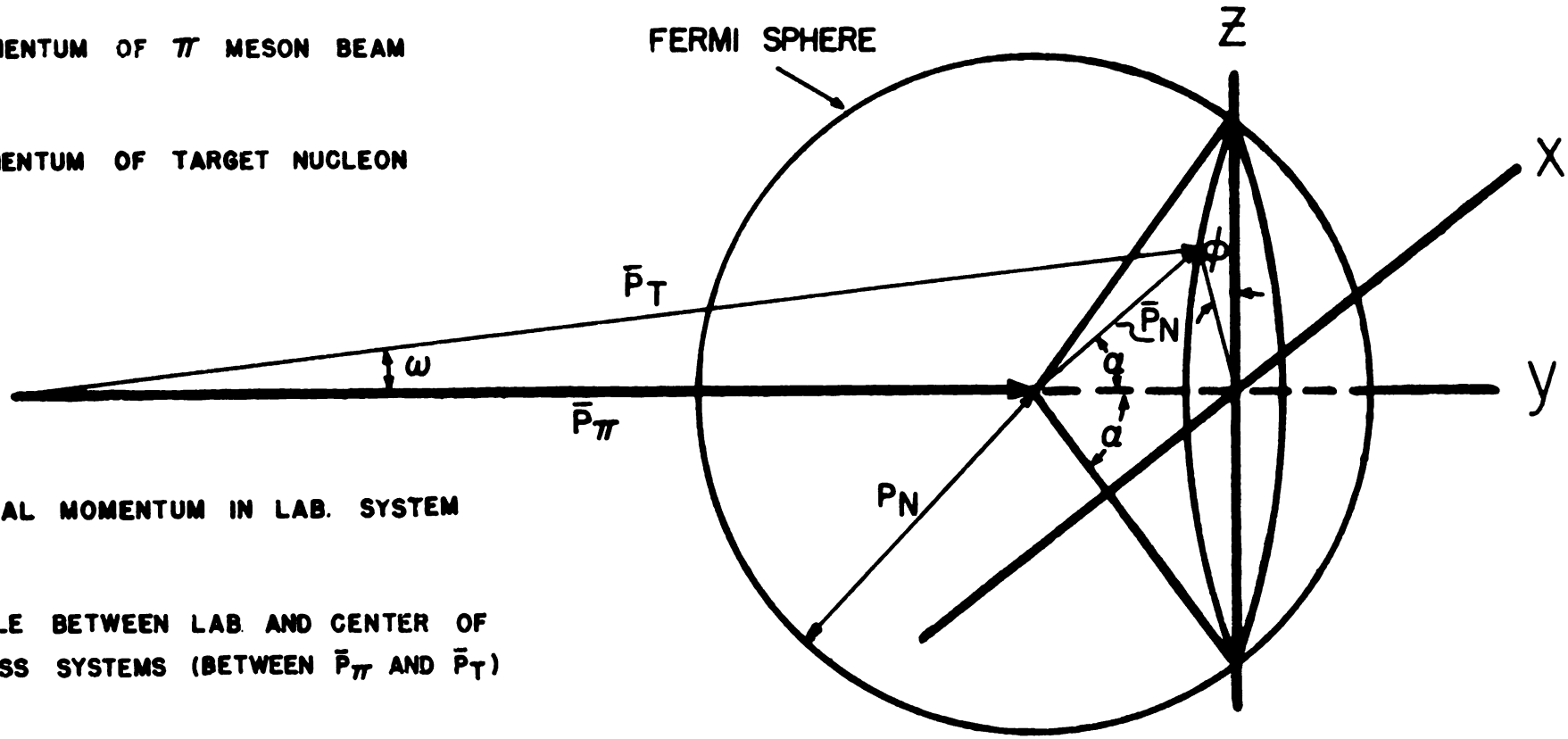

$\bar{P}_T$ - TOTAL MOMENTUM IN LAB. SYSTEM

ω - ANGLE BETWEEN LAB AND CENTER OF MASS SYSTEMS (BETWEEN $\bar{P}_\pi$ AND $\bar{P}_T$)

α - ANGLE BETWEEN $\bar{P}_\pi$ AND $\bar{P}_N$

FIG. 4 MOMENTUM DIAGRAM

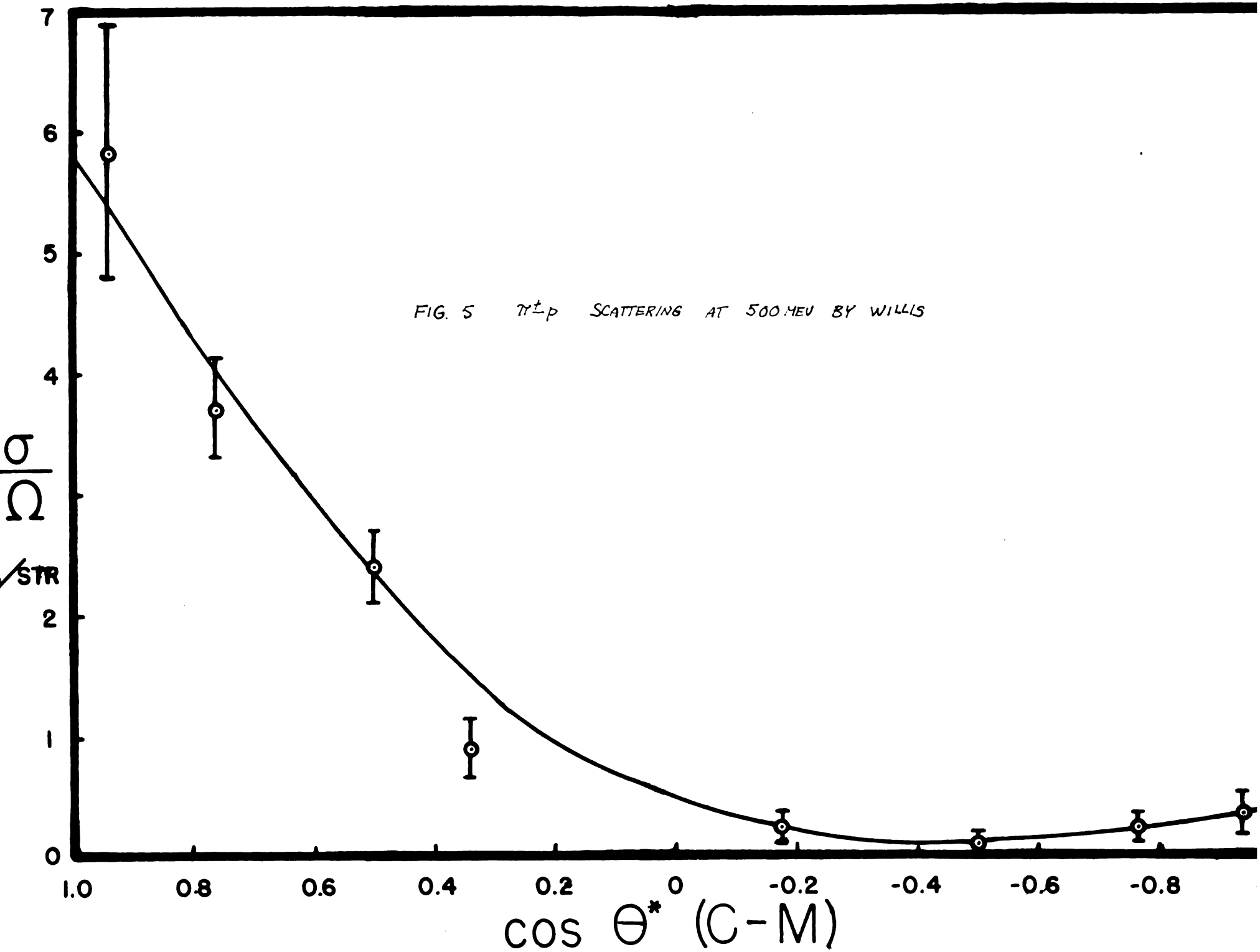

FIG. 5 $\pi^{\pm}p$ SCATTERING AT 500 MEV BY WILLIS

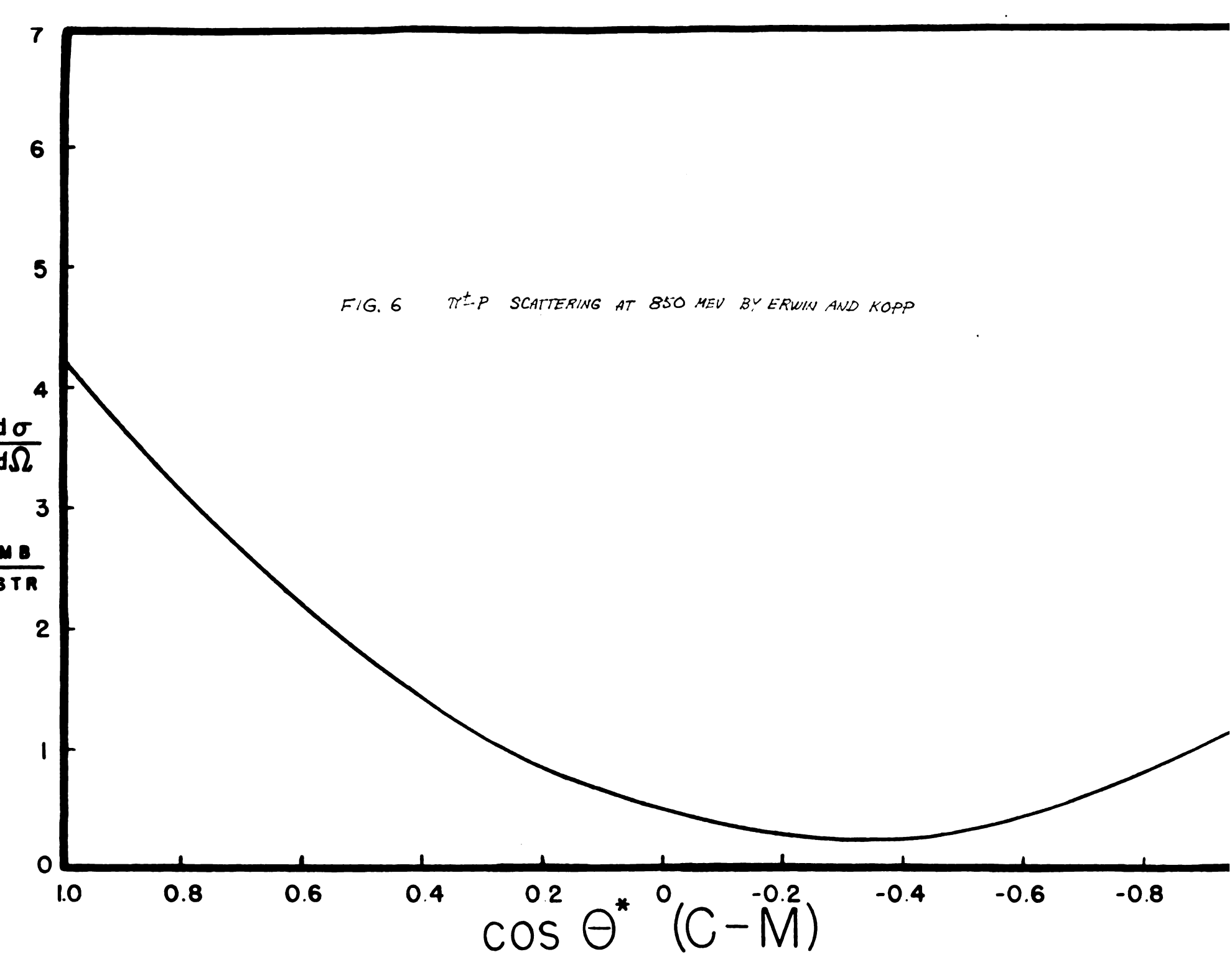
FIG. 6 $\pi^{\pm}$-P SCATTERING AT 850 MEV BY ERWIN AND KOPP
$\frac{d\sigma}{d\Omega}$
MB/STR
7
6
5
4
3
2
1
0
1.0
0.8
0.6
0.4
0.2
0
-0.2
-0.4
-0.6
-0.8
cos Θ^* (C-M)

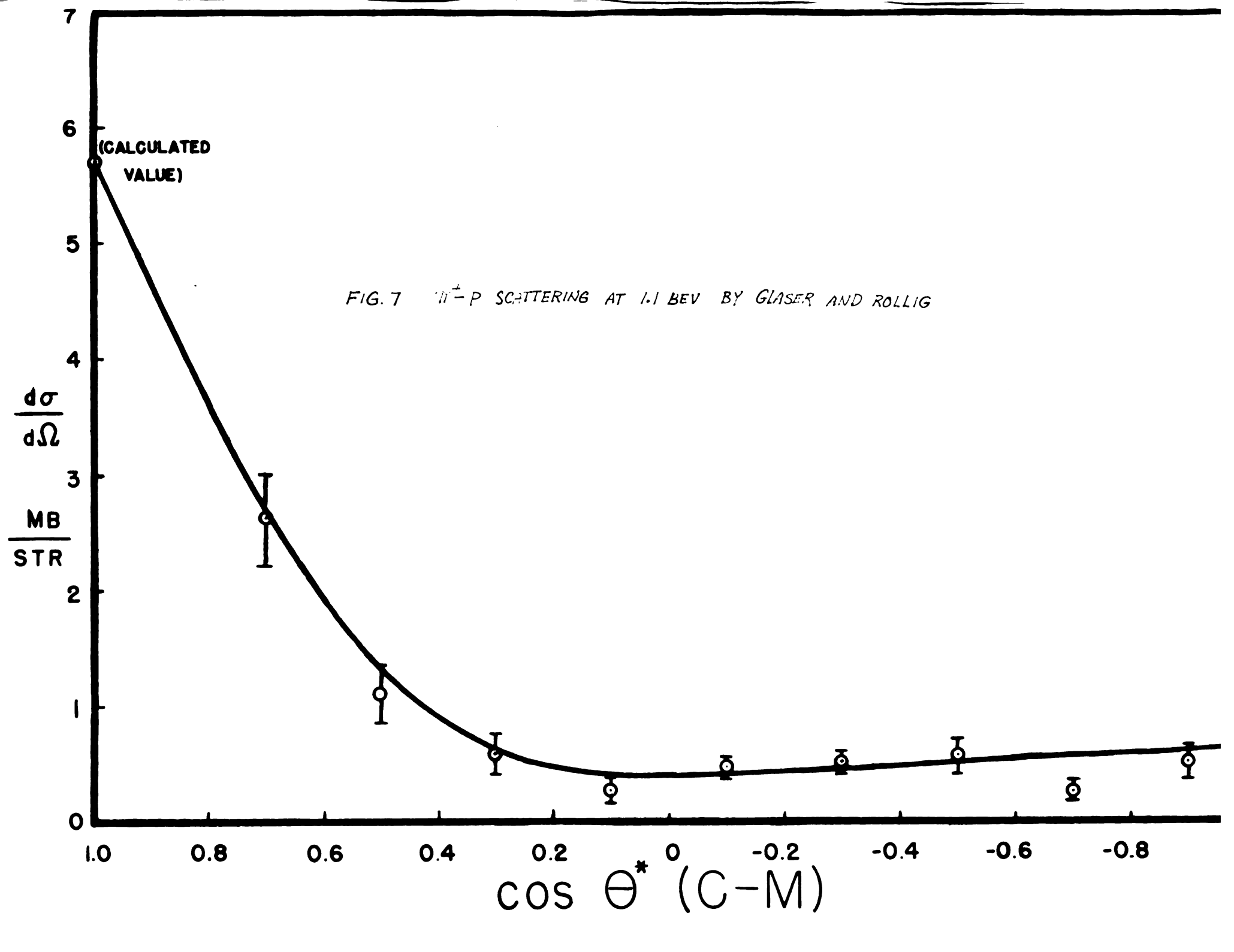

FIG. 7 $\pi^{\pm}$ P SCATTERING AT 1.1 BEV BY GLASER AND ROLLIG

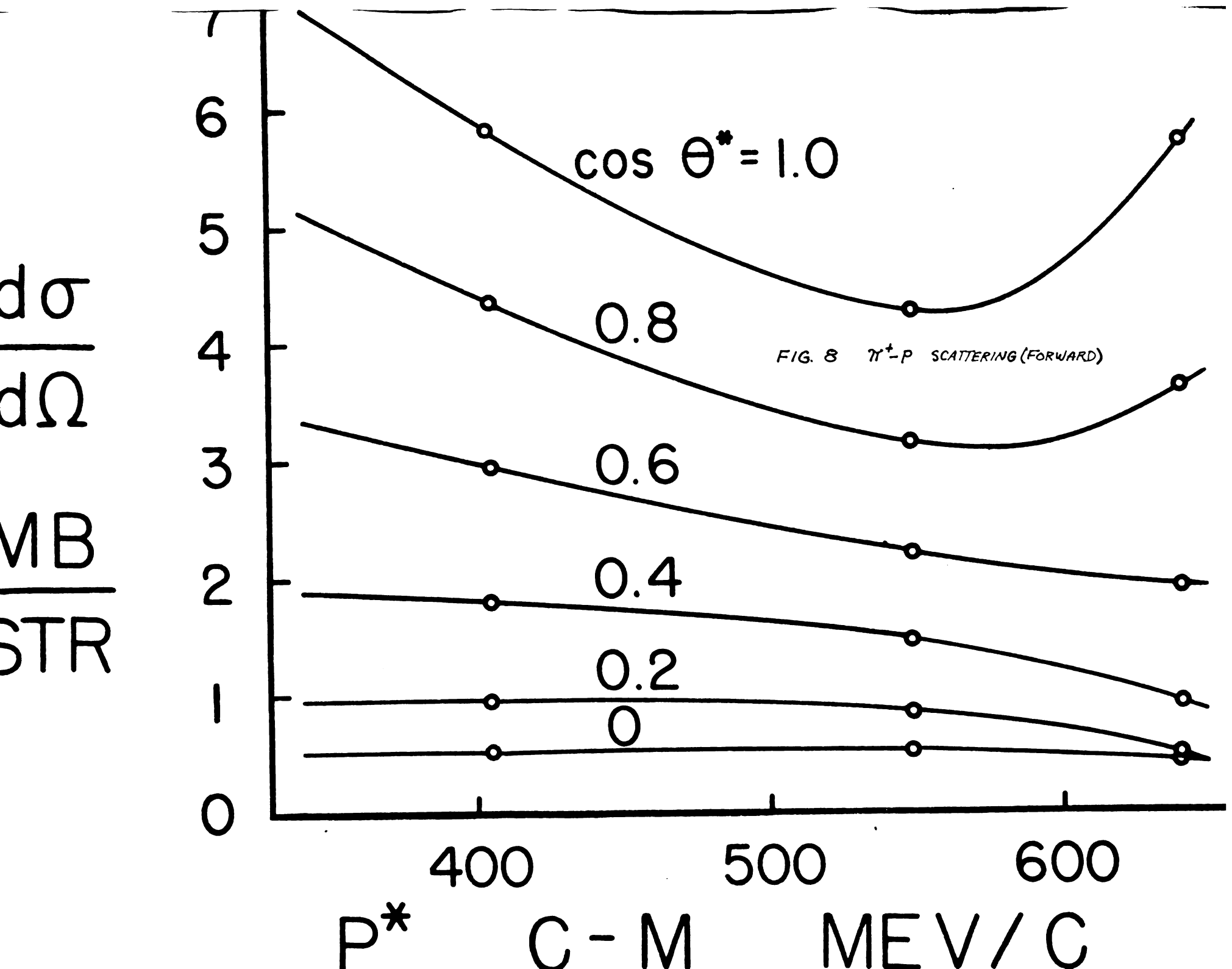

FIG. 8 π^+-P SCATTERING (FORWARD)

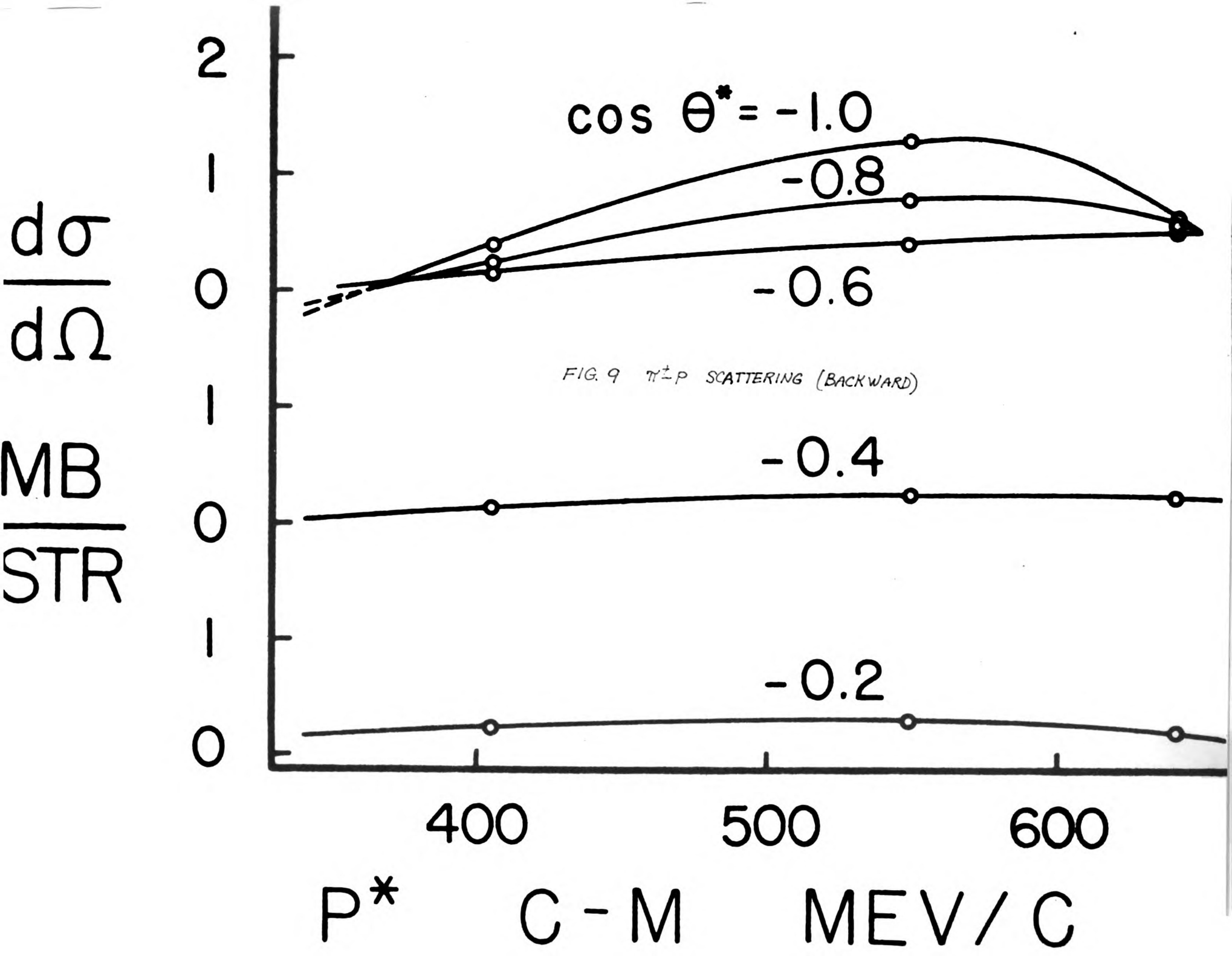

FIG. 9 $\pi^{\pm}p$ SCATTERING (BACKWARD)

500 mev[5], 850 mev[6], and 1.1 bev[7] as shown in figures 5, 6, and 7. The corresponding momenta available in the center of mass system are 405 mev/c, 549 mev/c, and 641 mev/c respectively. This is calculated from considering the Lorentz transformation of the momentum vector from the center of mass co-ordinate system to the laboratory co-ordinate system.

$$P^* = \gamma (P - \beta E) \tag{6}$$

where

$$\beta = (P_\pi + P_p) \div (E_\pi + E_p) \tag{7}$$

$$\gamma = (1 - \beta^2)^{-1/2} \tag{8}$$

From figures 5, 6, and 7, we can make a cross plot of $d\sigma/d\Omega$ vs P^* with cos θ^* as the parameter. The plots are shown in figures 8 and 9. From figures 8 and 9, we can determine the center of mass distribution of any (π^+,p) scattering, moving or stationary target once P^* is determined. Thus, for a particular point on the Fermi sphere, we can obtain a center of mass angular distribution by solving for P^* of that particular point.

Inorder to obtain P^* for a particular point on the Fermi sphere, we need only specify the angle α (see fig.4) that is related to the point. This is evident from equation 6, 8, and the following,

$$\beta = P_T \div \left(\sqrt{P_\pi^2 + m_\pi^2} + \sqrt{P_p^2 + m_p^2}\right) \tag{7a}$$

$$P_T = \left(P_\pi^2 + P_p^2 + 2 P_\pi P_p \cos\alpha\right)^{1/2} \tag{9}$$

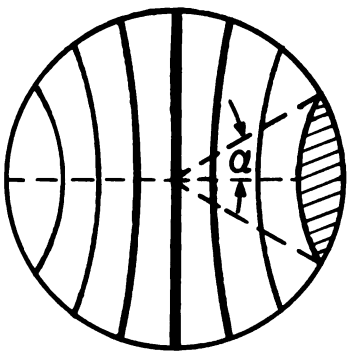

Figure 10 Dissection of Fermi Sphere.

For our choice of α's, let us first slice the Fermi sphere into eight sections as illustrated in figure 10. Again referring to figure 4, this is done by taking eight different values of α. The α's were chosen such that each center of mass angular distribution corresponding to the particular α will be weighted equally (equal solid angle involved). Table 3 lists the α's chosen and the corresponding cos α's, β's, P^*'s, ω's and P'_π's. The equations used to compute the variables are listed right below the Table. The variable P''_π will be explained later.

For each of the eight values of α listed in Table 3, we can determine a center of mass angular distribution by using figures 8 and 9. We must next consider transforming these eight angular distributions into the laboratory system. To transform to the laboratory system, let us again

Table 3.

P_π = 590 mev/c and P_p = 191 mev/c					
α(deg.)	cosα	β	P^* mev/c	ω(deg.)	P'_π mev/c
34.4	0.875	0.471	346	9.21	853
51.3	0.625	0.446	358	12.38	771
68.0	0.375	0.420	370	15.69	700
82.8	0.125	0.392	382	17.95	621
97.2	-0.125	0.361	398	19.58	545
112.0	-0.375	0.328	414	20.23	477
128.7	-0.625	0.291	433	19.15	403
145.6	-0.875	0.247	455	17.78	325

(6) $$P^* = \gamma (P - \beta E)$$

(7a) $$\beta = P_T \div \left(\sqrt{P_\pi^2 + m_\pi^2} + \sqrt{P_p^2 + m_p^2} \right)$$

(8) $$\gamma = (1 - \beta^2)^{-1/2}$$

(9) $$P_T = \left(P_\pi^2 + P_p^2 + 2 P_\pi P_p \cos\alpha \right)^{1/2}$$

(10) $$\sin\omega = P_p \sin\alpha \div P_T$$

(11) $$P'_\pi = \frac{-\beta m_p}{1-\beta^2} \pm \sqrt{\frac{\beta^2 m_p^2}{(1-\beta^2)^2} - \frac{\beta^2}{1-\beta^2}\left(m_p^2 - m_\pi^2\right)}$$

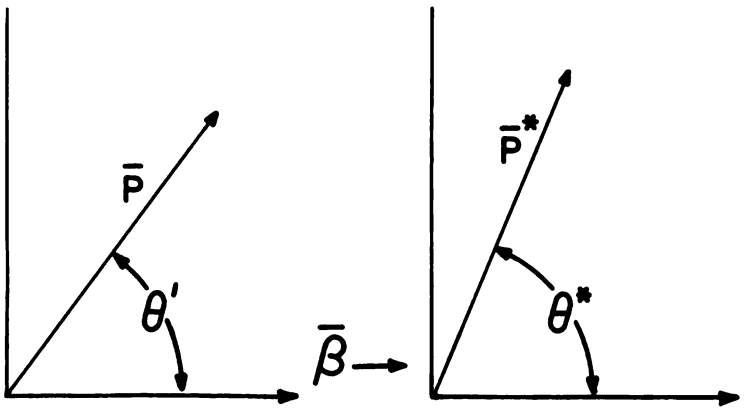

Figure 11.

consider the Lorentz transformation of the energy-momentum four vector.

(12) longitudinal $P\cos\theta' = \gamma(P^*\cos\theta^* + \beta E^*)$

(13) transverse $P\sin\theta' = P^*\sin\theta^*$

where θ' and θ^* are illustrated in figure 11. Dividing equation 12 by 13, we get

(14) $\tan\theta' = \sin\theta^* \div (\gamma\cos\theta^* + \beta E^*/P^*)$

We can now transform our center of mass angular distributions to the laboratory system by using equation 14.

However, by referring to figure 11, we notice that the angle θ' is measured with respect to the direction of ß. With a stationary target, this presents no difficulties since ß is along the same direction as the incident particle in the laboratory system. But with a moving target,

ß is in a different direction with the incident particle in the laboratory system. The desired angle "θ" is the angle between the direction of the incident particle and the scattered particle in the laboratory system.

To correct for this shift in angles, consider the diagram illustrated in figure 12. The primed co-ordinate system refers to the scattering system, the system which gives the angle θ'' with respect to the direction of ß. The unprimed co-ordinate system refers to the reference system, the system which gives the angle θ with respect to the incident pion beam in the laboratory system. We can write for the unit vectors $\bar{r}_1$ and $\bar{r}_2$,

$$(15) \quad \bar{r}_1 = \sin\omega\, \bar{i} + \cos\omega\, \bar{j} + 0\,\bar{k}$$

$$(16) \quad \bar{r}_2 = \sin\theta_\pi' \sin\phi'\, \bar{i} + \cos\theta_\pi'\, \bar{j} + \sin\theta_\pi' \cos\phi'\, \bar{k}$$

The actual scattering angle θ_π can now be obtained from the following expression,

$$(17) \quad \bar{r}_1 \cdot \bar{r}_2 = \cos\theta_\pi = \sin\omega \sin\phi' \sin\theta_\pi' + \cos\omega \cos\theta_\pi'$$

We shall now complete the dissection of the Fermi sphere. Cutting along the angle ϕ', we shall split each of the eight sections shown in figure 10 into four equal parts. For simplicity, let us choose for the angle ϕ'', the values 0°, 90°, 180°, and 270°. Equation 17 now simplifies to

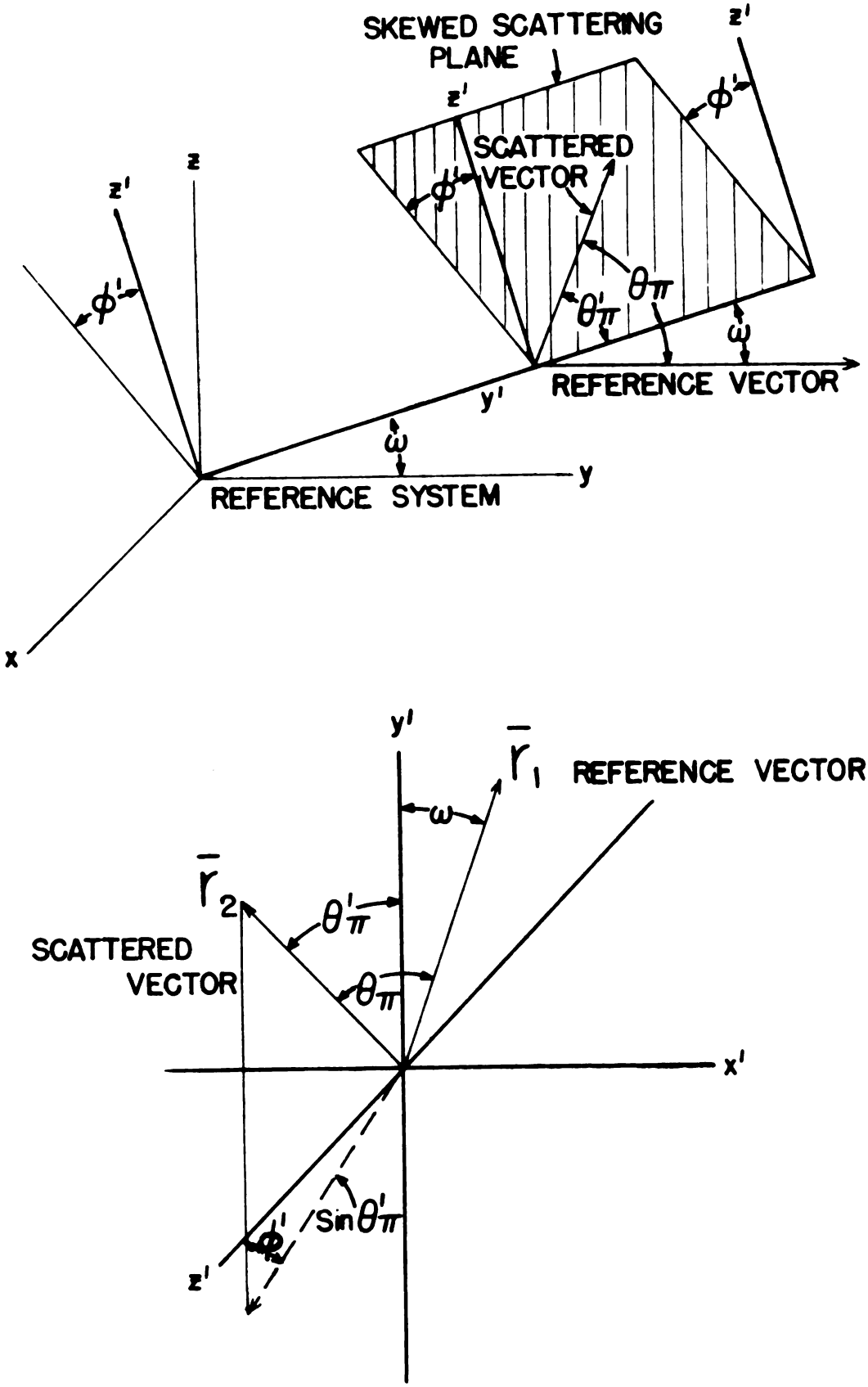
SKEWED SCATTERING PLANE
z'
z
z'
ϕ'
SCATTERED VECTOR
ϕ'
θ_π
θ'_π
ω
REFERENCE VECTOR
y'
ω
y
REFERENCE SYSTEM
x
y'
$\bar{r}_1$
REFERENCE VECTOR
ω
$\bar{r}_2$
θ'_π
SCATTERED VECTOR
θ_π
x'
ϕ'
$\sin\theta'_\pi$
z'

FIGURE 12

FIG. 13 KINEMATIC CURVES

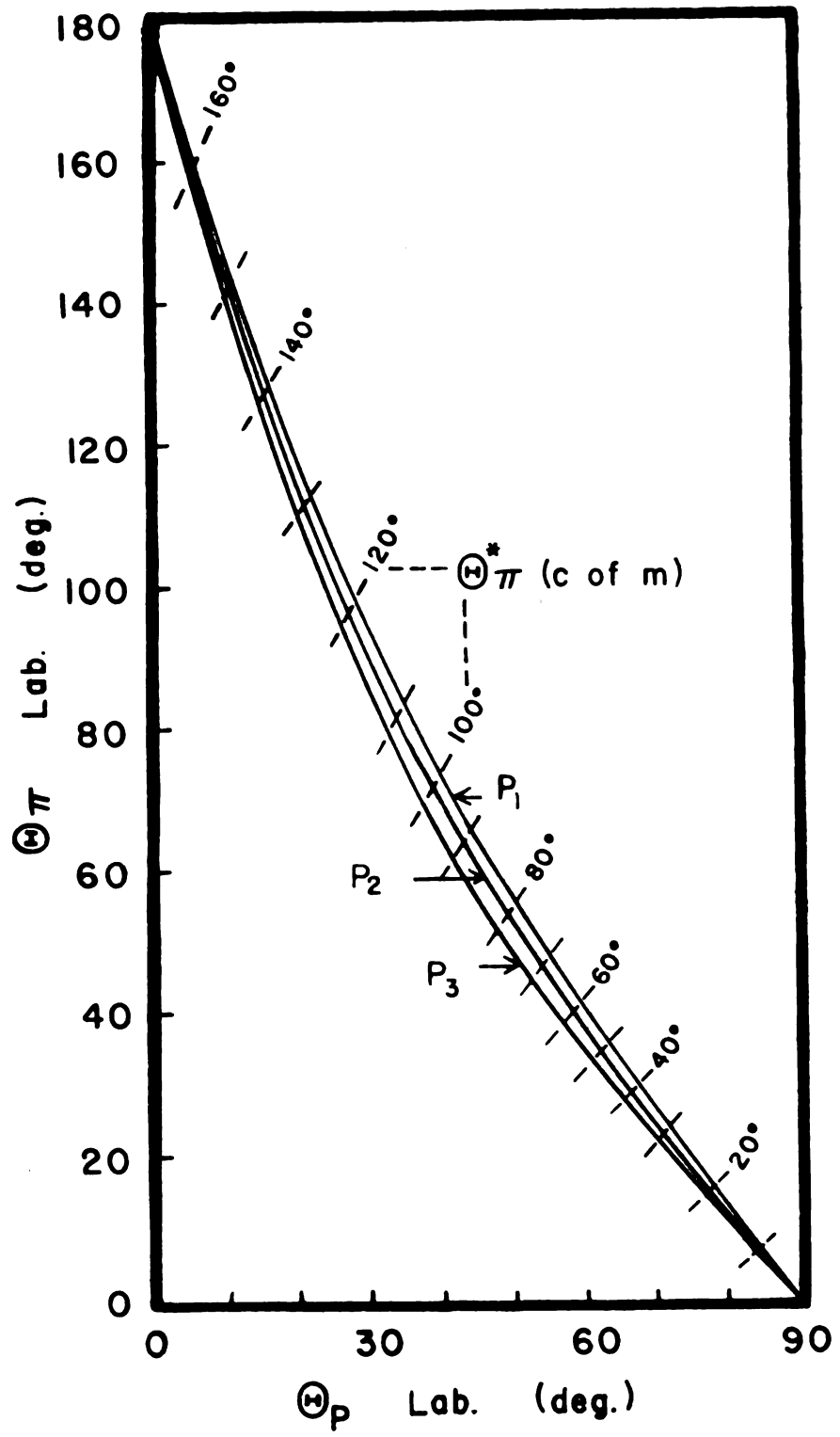

(18) $\phi' = 0^\circ, 180^\circ$ $\quad \cos\theta_\pi = \cos\omega \cos\theta_\pi'$

(19) $\phi' = 90^\circ$ $\quad \cos\theta_\pi = \cos(\theta_\pi' - \omega)$

(20) $\phi' = 270^\circ$ $\quad \cos\theta_\pi = \cos(\theta_\pi' + \omega)$

For each of the $d\sigma/d\Omega$ vs cos θ_π', we now have in its place four $d\sigma/d\Omega$ vs cos θ_π angular distributions.

Let us now return to equation 14 which transforms the angular distributions from the center of mass to the laboratory co-ordinate system. Instead of doing all the calculations using this equation, we shall make use of the already available kinematic curves shown in figure 13. These curves were calculated using equation 14, but for a stationary target[14]. The curves give a relationship between θ_π', θ_p', θ_π^*, and P_π. However, we can just as well think of the curves as a relationship between θ_π', θ_p', θ_π^*, and ß. This would make the curves adaptable to moving target scatterings. To utilize the kinematic curves, let us think of the collision with a moving target as one of an incident pion beam with momentum P_π' and a stationary target. P_π', of course, must be chosen such that ß is preserved.

(21) $\beta = P_\pi' \div \left(\sqrt{P_\pi'^2 + m_\pi^2} + m_p\right) = P_T \div \left(\sqrt{P_\pi^2 + m_\pi^2} + \sqrt{P_p^2 + m_p^2}\right)$

Values for P_π' are listed in Table 3. By using P_π', we are really using ß in disguise. Now we may adopt figure 13 for our computations.

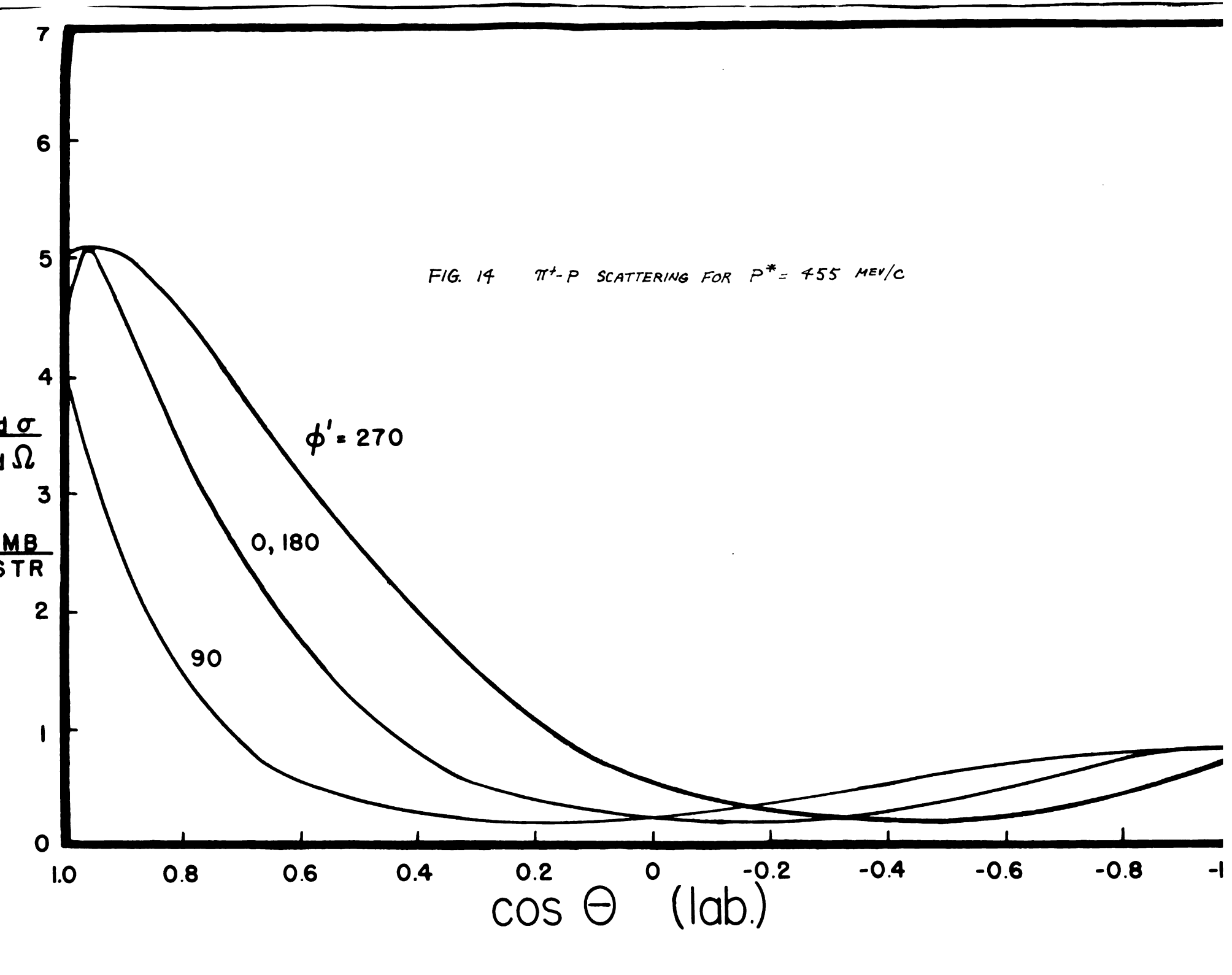
FIG. 14 π^+-P SCATTERING FOR P^* = 455 MEV/C
$\phi' = 270$
0, 180
90
$\frac{d\sigma}{d\Omega}$
MB/STR
7
6
5
4
3
2
1
0
1.0
0.8
0.6
0.4
0.2
0
-0.2
-0.4
-0.6
-0.8
cos Θ (lab.)

In detail, here is how the computations were done.

a. From figures 8 and 9, determine angular distributions for each of the P^*'s listed in Table 3.

b. For each of the P^*'s, transfer over to the laboratory system (θ'_π with respect to ß) using figure 13. First take a particular value of cos θ^*_π and note the corresponding value of $d\sigma/d\Omega$. From figure 13, find the cos θ'_π which corresponds to the value of cos θ^*_π and P'_π under consideration. This value of cos θ'_π will now correspond to the above value of $d\sigma/d\Omega$.

c. For each cos θ'_π, we have four corresponding values for cos θ_π ($\phi' = 0^\circ$, 90°, 180°, & 270°). These are calculated from equations 18, 19, and 20. Values of ω may be obtained from Table 3. An example of the angular distributions with respect to θ for $\alpha = 145.6^\circ$ and $\phi' = 0^\circ$, 90°, 180°, and 270° are shown in figure 14.

d. We now have 32 angular distributions from the eight values of α and the four values of ϕ'. The net effect is just the average of them all. The next step is to add up the 32 distributions and divide by 32.

The resultant curve is shown as the solid curve in figure 15. The dotted curve represents the angular distribution for a stationary target at a pion laboratory momentum of 590 mev/c. The stationary target curve was obtained by

a. Finding the center of mass angular distribution

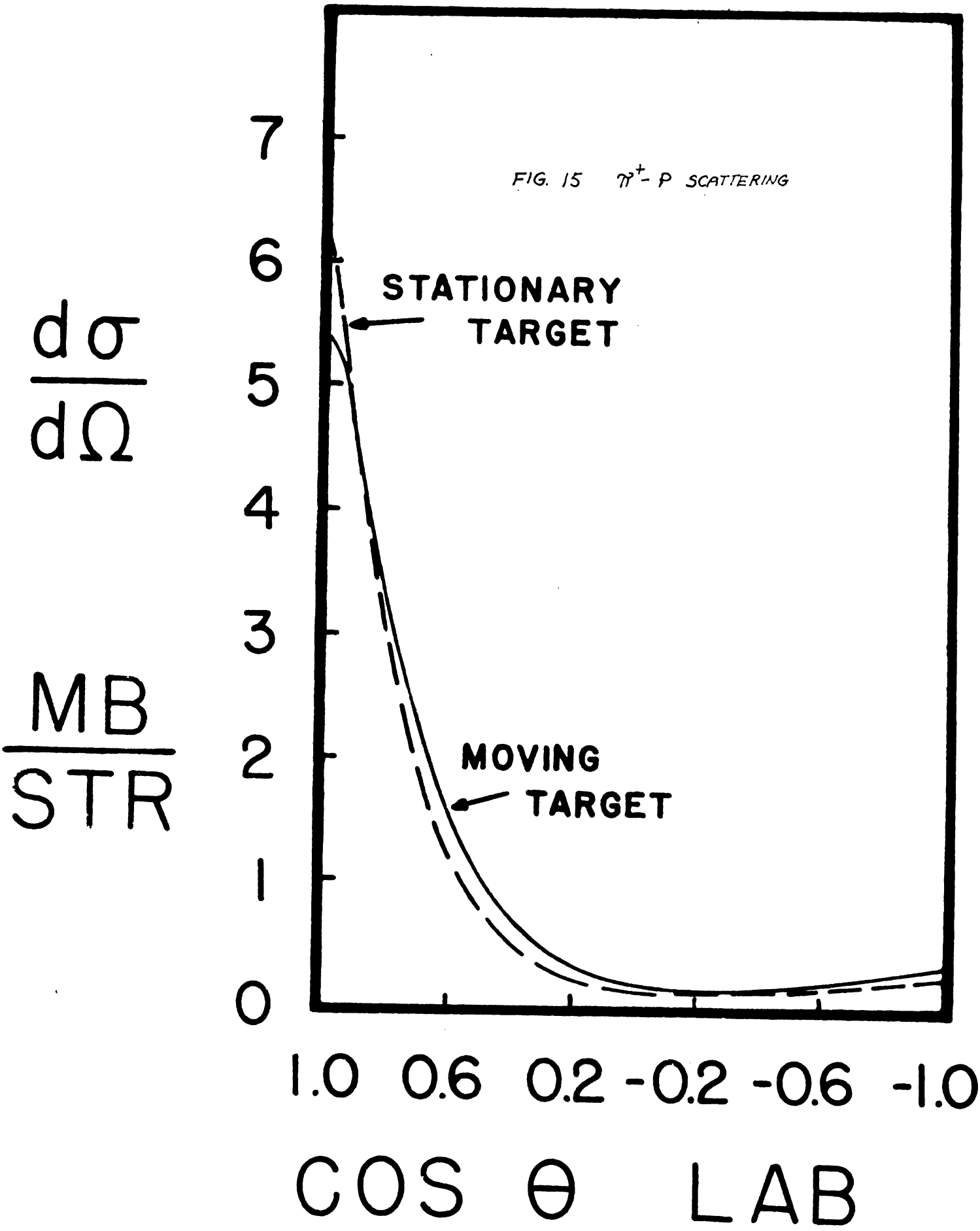
FIG. 15 π^+- P SCATTERING
STATIONARY TARGET
MOVING TARGET
$\frac{d\sigma}{d\Omega}$
$\frac{MB}{STR}$
0
1
2
3
4
5
6
7
1.0 0.6 0.2 -0.2 -0.6 -1.0
COS θ LAB

FIG. 16 π^- P SCATTERING

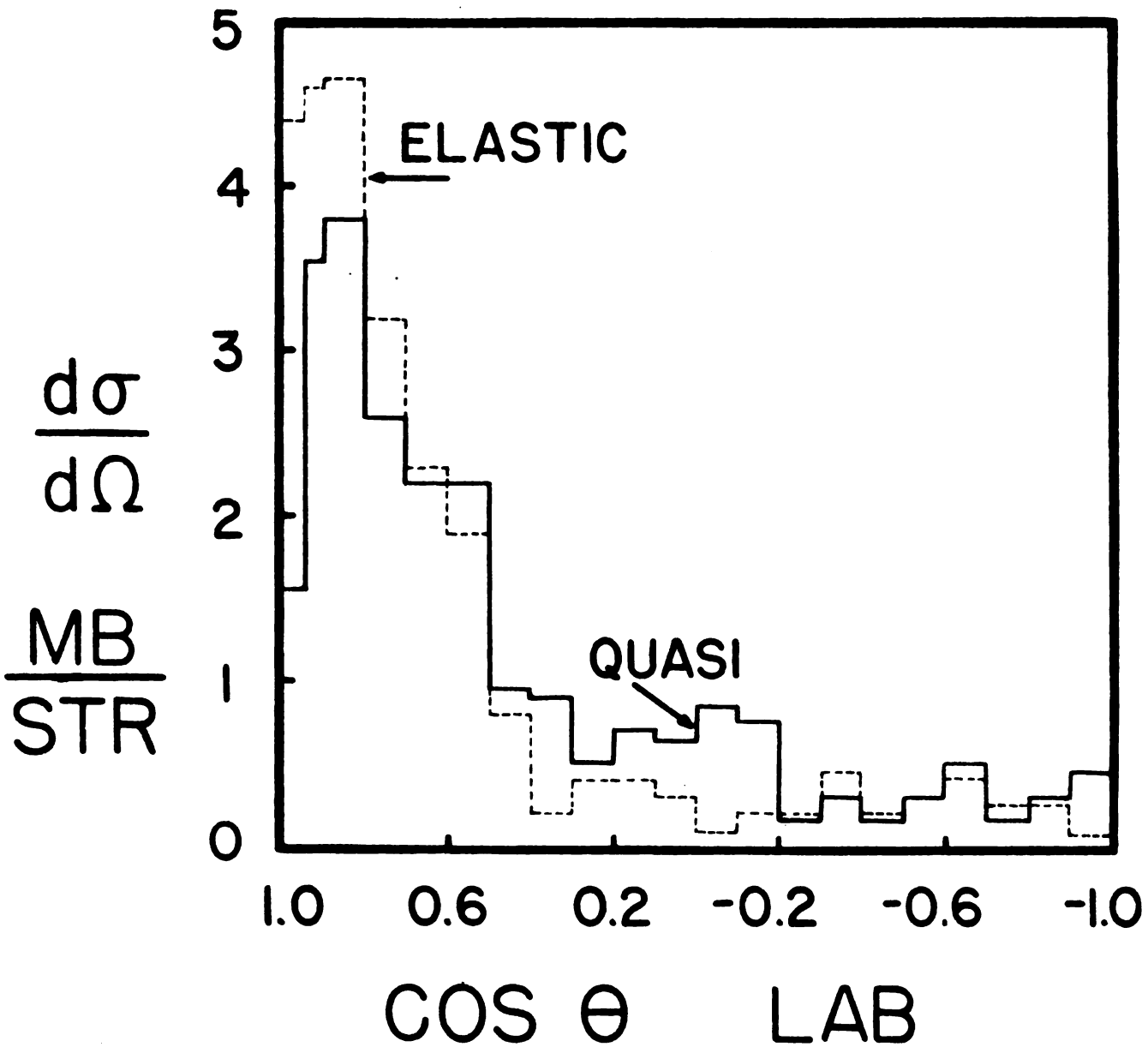

from figures 8 and 9 ($P^* = 387$ mev/c).

b. Transferring to the laboratory system using the kinematic curves in figure 13. ($\theta = \theta'$ since $\omega = 0$ for a stationary target)

As can be seen from figure 15, there is very little difference between the two distributions.

As an experimental check on the results, we made use of the elastic (stationary target) and quasi-elastic (moving target) data mentioned in section II. Angular distributions were calculated for the two and are shown in figure 16. The curves are in good agreement with the predicted results of stationary and moving target angular distributions.

B. Diffraction Scattering.

Now that we have corrected for the moving target, the only thing left is the correction for the diffraction scattering from the carbon nucleus. Assuming that the incident meson wave sees the carbon nucleus as a black sphere, we have for the angular distribution,[15]

$$(22) \qquad \frac{d\sigma(diff.)}{d\Omega} = \frac{\sigma(diff.)}{i\pi}\left[\frac{J_1(k^* R \sin\theta^*)}{\sin\theta^*}\right]^2$$

where $k^* = h/P^*$ and $R = r_o A^{1/3}$ are the wave number and radius of the nucleus respectively. The deflections, as mentioned before, consist of both the (π^-,n) and the diffraction scatterings. Therefore, before we can compare the (π^-,n) and (π^+,p) interactions, we must add the diffraction effect to the transformed (π^+,p) scattering or subtract the diffraction effect from the deflections. We shall do the former.

At first one might expect that since there are six neutrons and six protons inside a carbon nucleus, we can simply write

$$(23) \qquad \frac{d\sigma(deflection)}{d\Omega} = \frac{d\sigma(diffraction)}{d\Omega} + 6\frac{d\sigma(\pi^-,n)}{d\Omega}$$

However, there is the problem that some of the nucleons are shielding the others which will reduce the factor six being used above. To obtain the correct factor, we turn to the (π^-,p) data listed in Table 1. We are reasonably sure in this case that we are able to distinguish between

an elastic event (free proton) and a quasi-event (proton bound inside a carbon nucleus). In propane (C_3H_8), if there were no shielding effects, we would expect a 8/18 ratio of elastics to quasi-elastics. The actual ratio was 298/369, indicating some shielding effects. Taking this into consideration, the relation

(24) $\quad 8/3m = 298/369$

should hold where "m" is the effective number of unshielded protons (or neutrons) inside the carbon nucleus. We can now write after solving for "m" in equation 24,

(25) $$\frac{d\sigma(\text{defl.})}{d\Omega} = \frac{d\sigma(\text{diff.})}{d\Omega} + 3.3\,\frac{d\sigma(\pi^-,n)}{d\Omega}$$

Or if charge symmetry is to hold, we must have

(26) $$3.3\,\frac{d\sigma(\pi^-,n)}{d\Omega} = \frac{d\sigma(\text{defl.})}{d\Omega} - \frac{d\sigma(\text{diff.})}{d\Omega} = 3.3\,\frac{d\sigma(\pi^+,p)}{d\Omega}$$

In equation 22, there are still two unknown constants, σ(diff.) and the radius parameter r_o to be determined. By trial and error methods, σ_i/π = 25 mb/str and $r_o = 1.1 \times 10^{-13}$ cm. were found to give the best results. Equation 22 can now be written as

(27) $$\frac{d\sigma(\text{diff.})}{d\Omega} = 25\left[\frac{J_1(7.12\sin\theta^*)}{\sin\theta^*}\right]^2$$

Values of the $d\sigma$(diff.)/$d\Omega$ curve were only taken to the first minimum (around 33°).

Rewriting equation 26, we have

(28) $$\frac{d\sigma(\text{defl.})}{d\Omega} = 3.3\,\frac{d\sigma(\pi^+,p)}{d\Omega} + \frac{d\sigma(\text{diff.})}{d\Omega}$$

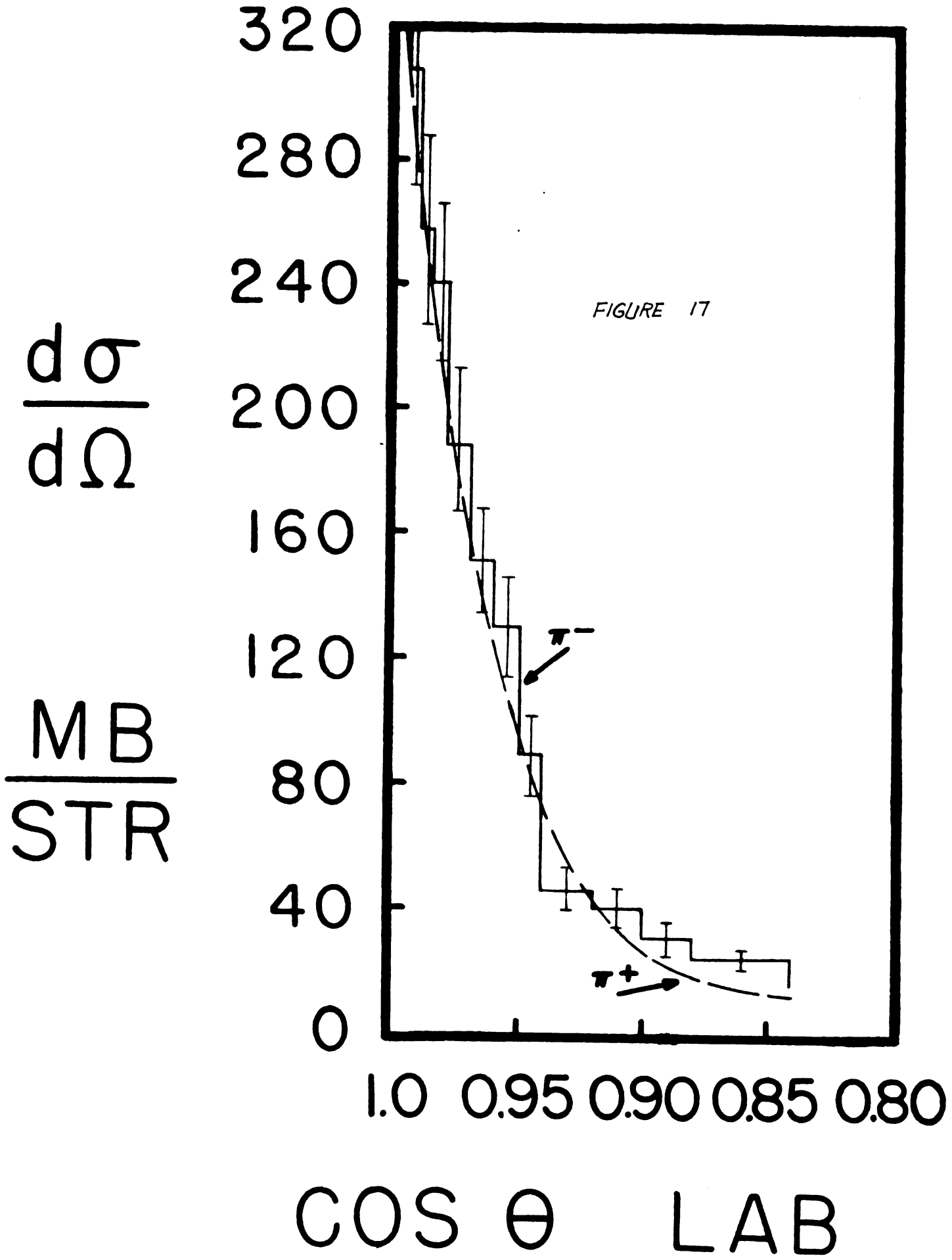
320
280
240
200
160
120
80
40
0
dσ/dΩ
MB/STR
π⁻
π⁺
1.0
0.95
0.90
0.85
0.80
COS θ LAB

FIGURE 17

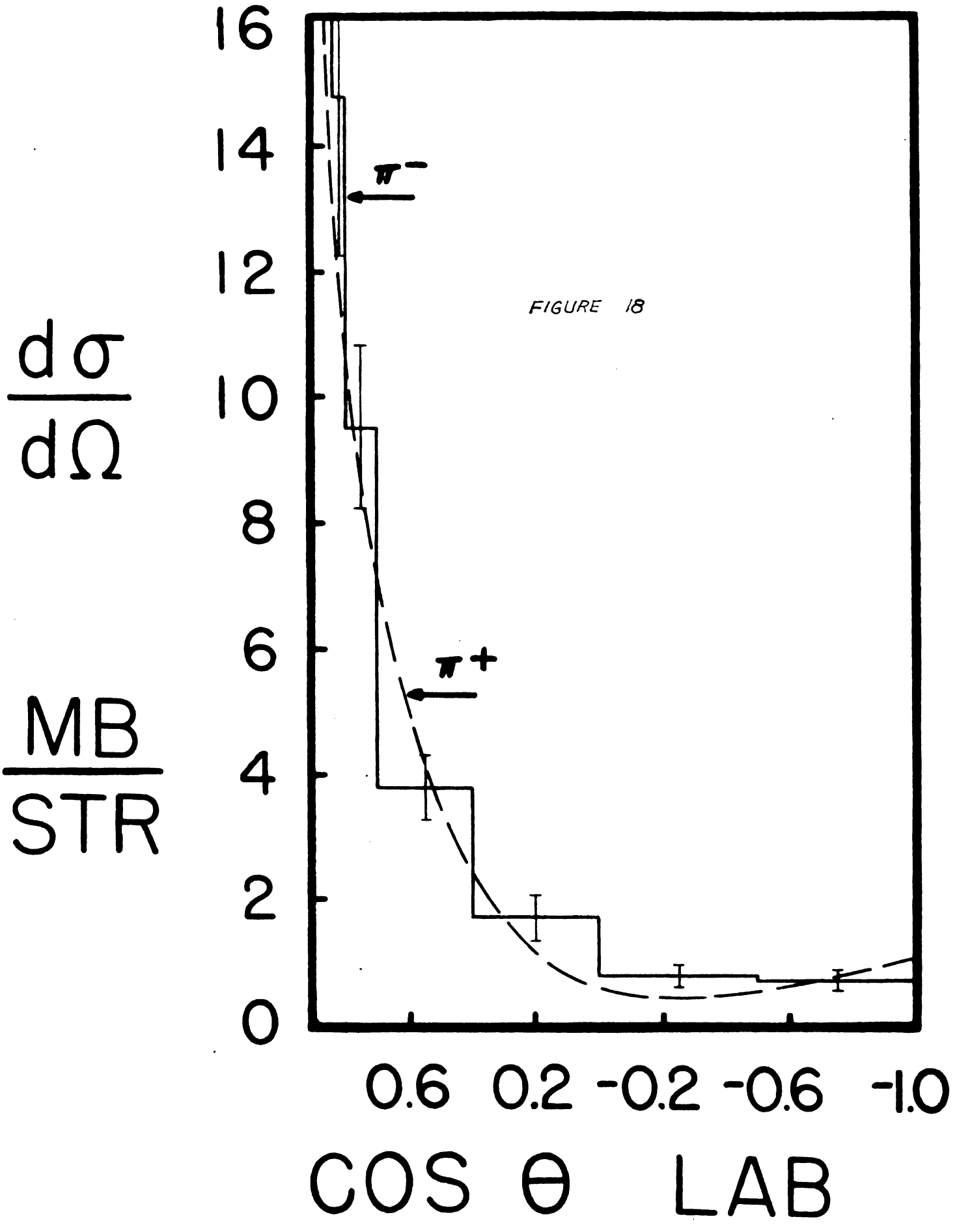

FIGURE 18

as the condition for the validity of charge symmetry. The observed $d\sigma$(defl.)/$d\Omega$ and the calculated value of 3.3 $d\sigma(\pi^+,p)/d\Omega$ + $d\sigma$(diff.)/$d\Omega$ are shown in figures 17 and 18 as the dashed curve and histogram respectively. A χ^2 test was applied to the curves, the result being ϵ(probability) = 0.054 for the entire curve and a ϵ(probability) = 0.20 for the part of the curve corresponding to laboratory angles greater than 33°. A χ^2 test with a ϵ(probability) of greater than 0.01 is sufficient for one not to reject a hypothesis. The results to our test thus gives us close enough agreement for us to say that charge symmetry has not been violated. As expected, the fit for laboratory angles greater than 33° is better than the fit at smaller angles where we had to apply the black sphere model to correct for the diffraction effect. It is also interesting to note that the value of 1.1 x 10^{-13} cm. for the radius parameter is in good agreement with the Stanford[16] determination of r_o (1.07 x 10^{-13} cm.).

IV CONCLUSION

Two immediate remarks can be made. One is that a moving target does not change the angular distribution appreciably. This is illustrated in figures 15 and 16. The other is that charge symmetry is not violated in the (π^-,n) and (π^+,p) scatterings. This is illustrated in figures 17 and 18. A closer look at figure 17 would also suggest that a better fit could be made in the region from cos θ equal 0.82 to 0.92. A smaller value for the radius parameter r_o accomplishes this. However, a smaller r_o also swings the curve off in the region around cos θ equal 0.98. It was decided that the black sphere approximation made earlier for the nucleus was responsible for this. To obtain more precise results, a model of the nucleus with a diffuse edge must be considered.

APPENDIX

ANALYSIS SCHEME FOR THE MEASUREMENT OF SPACE ANGLES

After obtaining the data, the problem is how to compute the space angle from the films taken. As mentioned before, the pictures were taken by two mutually perpendicular cameras in order to obtain a stereoscopic view of the events. The main difficulty is that the cameras must be placed at a finite distance away from the chamber. As a consequence, the events seen on the films represent the conical projections of the true space events. In this section, we shall set up an analysis to measure the space angle between two intersecting vectors in space knowing in the mutually orthogonal side and bottom views, the conically projected angles, the co-ordinates of the vertices of the conically projected angles, and the co-ordinates of the points of projection. Correction factors for the change in index of refraction in traveling from propane to air are taken into consideration. A coplanarity test for events with three prongs (three intersecting vectors in space) is also considered. The analysis scheme has been set up in particular to solve for space angles in a (π^-,p) scattering experiment, but may be applied to a (π^-,n) scattering and other types of problems too.

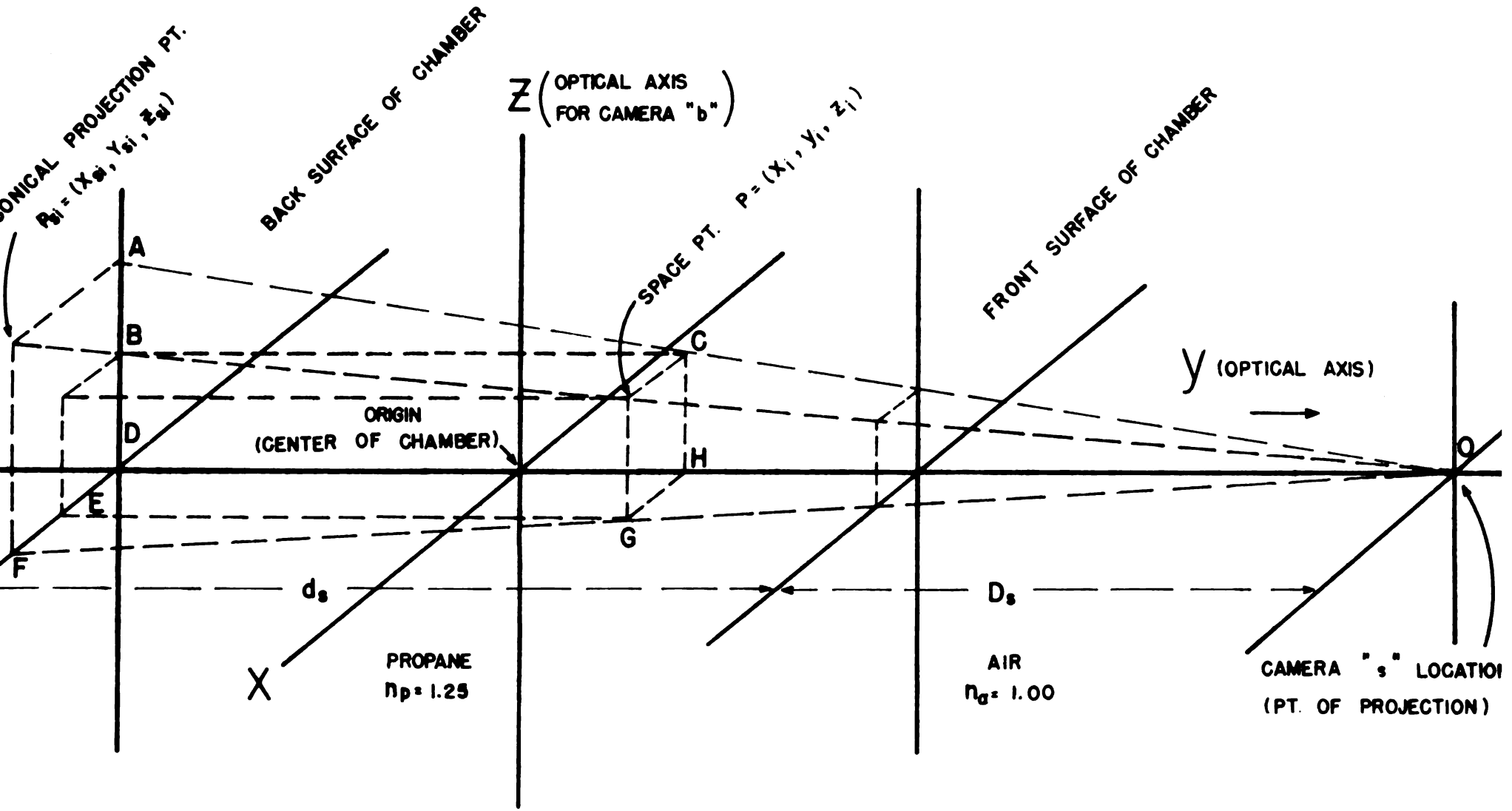
ONICAL PROJECTION PT.
$P_{si} = (X_{si}, Y_{si}, Z_{si})$
BACK SURFACE OF CHAMBER
Z (OPTICAL AXIS FOR CAMERA "b")
SPACE PT. $P = (X_i, Y_i, Z_i)$
FRONT SURFACE OF CHAMBER
y (OPTICAL AXIS)
A
B
C
D
E
F
G
H
O
ORIGIN
(CENTER OF CHAMBER)
d_s
D_s
X
PROPANE
$n_p = 1.25$
AIR
$n_a = 1.00$
CAMERA "s" LOCATIO
(PT. OF PROJECTION)

FIGURE 1A

In figure 1A is shown one view of the cameras. In practice what is usually done is to mark the surface of the chamber with identification markers a specified distance apart. These markers will show up in the films taken and can be used to calibrate the actual size of the events. The film will then be projected back onto a screen to about twice the size between the original markers. This is illustrated in figure 1A where the back side of the chamber now represents the conically projected plane. Now we are ready to proceed to derive an expression for the space angle θ in terms of measurements made on the conically projected plane (the screen) and the co-ordinates of the points of projection.

A. Derivation of Equations for the Orthogonally Projected Angles.

From figure 1A, the following sets of triangles are similar.

(a) $\triangle ADO$ and $\triangle CHO$

(b) $\triangle DFO$ and $\triangle HGO$

Let us take as our space point (x_i, y_i, z_i) and as our conically projected point (X_{Si}, Y_{Si}, Z_{Si}). The distances are then as follows:

(c) $AD = Z_{Si}$

(d) $CH = z_i$

(e) $GH = x_i$

(f) $FD = X_{si}$

(g) $DO = D_s + d_s/n_p$

(h) $HO = D_s + (d_s/2 - y_i)/n_p$

where n_p represents the index of refraction for propane. The last two distances DO and HO are corrected for the change in optical path due to a change in the index of refraction in traveling from air to propane. Since corresponding sides are proportional in similar triangles, we have from the relations (a) and (b),

$$\text{(1A)} \qquad \begin{aligned} AD/DO &= CH/HO \\ FD/DO &= GH/HO \end{aligned}$$

or rewriting as

$$\text{(2A)} \qquad \begin{aligned} Z_{si}/(D_s + d_s/n_p) &= z_i/\left[D_s + \tfrac{1}{n_p}\left(\tfrac{d_s}{2} - y_i\right)\right] \\ X_{si}/(D_s + d_s/n_p) &= x_i/\left[D_s + \tfrac{1}{n_p}\left(\tfrac{d_s}{2} - y_i\right)\right] \end{aligned}$$

Next define

$$\text{(3A)} \qquad Y'_{si} = \frac{1}{n_p}\left(\frac{d_s}{2} - y_i\right)$$

We then have

$$\text{(4A)} \qquad \begin{aligned} Z_{si} &= z_i\left(\frac{D_s + d_s/n_p}{D_s + Y'_{si}}\right) \\ X_{si} &= x_i\left(\frac{D_s + d_s/n_p}{D_s + Y'_{si}}\right) \end{aligned}$$

Let us now take two arbitrary space points (x_1, y_1, z_1) and (x_2, y_2, z_2) and their corresponding conical projection (X_{s2}, Y_{s2}, Z_{s2}) and (X_{s1}, Y_{s1}, Z_{s1}). These two points form a vector $\bar{r}_{12}$ in three space, and their corresponding conical projections form a vector in plane "s". The vector being

$(X_{S2}-X_{S1},\ 0,\ Z_{S2}-Z_{S1})$. The tangent of the angle θ_s' that this vector makes with the x axis in plane "s" is

$$\text{(5A)} \qquad \tan\theta_s' = (Z_{S2} - Z_{S1}) \div (X_{S2} - X_{S1})$$

Substituting equation 4A into 5A and simplifying, we have

$$\text{(6A)} \qquad \tan\theta_s' = \frac{(z_2 - z_1) + z_2\left(\dfrac{D_s + d_s/n_p + Y_{S1}'}{D_s + d_s/n_p + Y_{S2}'} - 1\right)}{(x_2 - x_1) + x_2\left(\dfrac{D_s + d_s/n_p + Y_{S1}'}{D_s + d_s/n_p + Y_{S2}'} - 1\right)}$$

Simplifying the term in brackets,

$$\text{(7A)} \qquad \left(\frac{D_s + d_s/n_p + Y_{S1}'}{D_s + d_s/n_p + Y_{S2}'} - 1\right) = \frac{y_2 - y_1}{n_p D_s + d_{s/2} - y_2}$$

Next define

$$\text{(8A)} \qquad A = (n_p D_s + d_s/2 - y_2)^{-1}$$

We may now rewrite tan θ_s' as

$$\text{(9A)} \qquad \tan\theta_s' = \frac{(z_2 - z_1) \div (x_2 - x_1) + z_2 A (y_2 - y_1) \div (x_2 - x_1)}{1 + x_2 A (y_2 - y_1) \div (x_2 - x_1)}$$

But $(z_2-z_1)/(x_2-x_1)$ is just the tangent of the orthogonally projected angle θ_s'' in plane "s*" and $(y_2-y_1)/x_2-x_1)$ is just the tangent of the orthogonally projected angle θ'' in plane "b*" (XY plane). The star "*" denotes the orthogonally projected plane as contrasted with the conical plane without the star. We may now write tan θ_s' as

$$\text{(10A)} \qquad \tan\theta_s' = (\tan\theta_s'' + z_2 A \tan\theta_b'') \div (1 + x_2 A \tan\theta_b'')$$

Next to simplify the expression $z_2 A$ and $x_2 A$ using equation 2A.

$$x_2 / X_{S2} = [A(n_p D_s + d_s)]^{-1}$$

$$\text{(11A)} \qquad z_2 / Z_{S2} = [A(n_p D_s + d_s)]^{-1}$$

Therefore,

$$\chi_2 A = X_{S2} / (n_p D_s + d_s)$$

(12A)

$$\gamma_2 A = Z_{S2} / (n_p D_s + d_s)$$

Taking equation 10A and rewriting in terms of tan θ"

$$\tan \theta_s'' = \tan \theta_s' + \tan \theta_b'' (\chi_2 A \tan \theta_s' - \gamma_2 A)$$

(13A)

$$\tan \theta_s'' = \tan \theta_s' + \tan \theta_b'' \left[\frac{X_{S2}}{d_s + n_p D_s} \tan \theta_s' - \frac{Z_{S2}}{d_s + n_p D_s} \right]$$

Let

(14A) $$A' = \frac{1}{n_p D_s + d_s} (X_{S2} \tan \theta_s' - Z_{S2})$$

Therefore,

(15A) $$\tan \theta_s'' = \tan \theta_s' + A' \tan \theta_b''$$

Let us now turn to the XY plane "b" where our other camera is located. The situation in plane "b" is exactly analogous to that in plane "s" and all our equations would be correct if we would change our subscripts "s" to "b" or "b" to "s" and our Z's to Y's or Y's to Z's. Equations 14A and 15A could now be written as

(16A) $$B' = \frac{1}{n_p D_b + d_b} (X_{b2} \tan \theta_b' - Z_{b2})$$

(17A) $$\tan \theta_b'' = \tan \theta_b' + B' \tan \theta_s''$$

Equations 15A and 17A can now be solved explicitly for θ_s'' and θ_b'' (two equations in two unknowns). The result being

$$\tan \theta_s'' = (\tan \theta_s' + A' \tan \theta_b') \div (1 - B'A')$$

(18A) $$\tan \theta_b'' = (\tan \theta_b' + B' \tan \theta_s') \div (1 - B'A')$$

We now have explicit expressions for our orthogonally projected angles in terms of measurable quantities - θ_s', θ_b', X_{s2}, Z_{s2}, X_{b2}, Z_{b2} and the constants n_p, D_s, and D_b.

B. Correction for Beam Angle.

It should be noted that the angles we have referred to so far are all measured with respect to the x axis. In a usual scattering experiment what we are interested in is the angle the scattered particle makes with the incident beam of bombarding particles. This beam is usually making a small angle with the x axis and must be corrected for. From the well known trigonometric formula for the sum of tangents of angles,

$$\text{(19A)} \qquad \begin{aligned} \tan\theta_b &= \left(\tan\theta_b'' - \tan\Omega_b'\right) \div \left(1 + \tan\Omega_b' \tan\theta_b'' + \tan\Omega_s' \tan\theta_s''\right) \\ \tan\theta_s &= \left(\tan\theta_s'' - \tan\Omega_s'\right) \div \left(1 + \tan\Omega_b' \tan\theta_b'' + \tan\Omega_s' \tan\theta_s''\right) \end{aligned}$$

where ' is the beam angle (angle it makes with the x axis). Making the assumption that the beam angle is always very small, we have

$$\text{(20A)} \qquad \begin{aligned} \tan\theta_b &= \left(\tan\theta_b'' - \Omega_b'\right) \div \left(1 + \Omega_b' \tan\theta_b'' + \Omega_s' \tan\theta_s''\right) \\ \tan\theta_s &= \left(\tan\theta_s'' - \Omega_s'\right) \div \left(1 + \Omega_b' \tan\theta_b'' + \Omega_s' \tan\theta_s''\right) \end{aligned}$$

as our true orthogonally projected angle with respect to the beam.

The tangent of the space angle can now be written as

$$\text{(21A)} \qquad \tan\theta = \left(\tan^2\theta_b + \tan^2\theta_s\right)^{1/2}$$

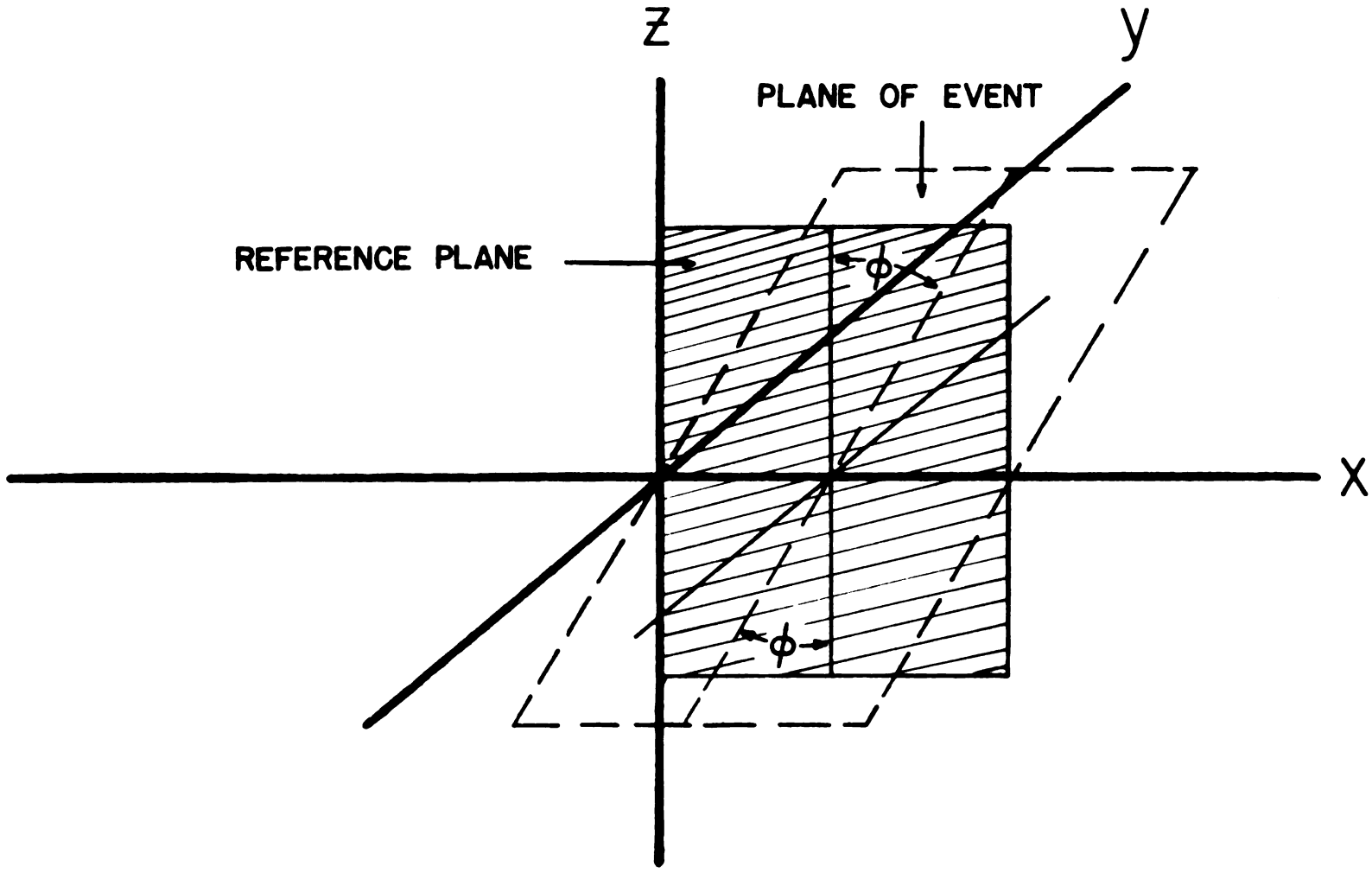

FIGURE 2A

FIGURE 3A

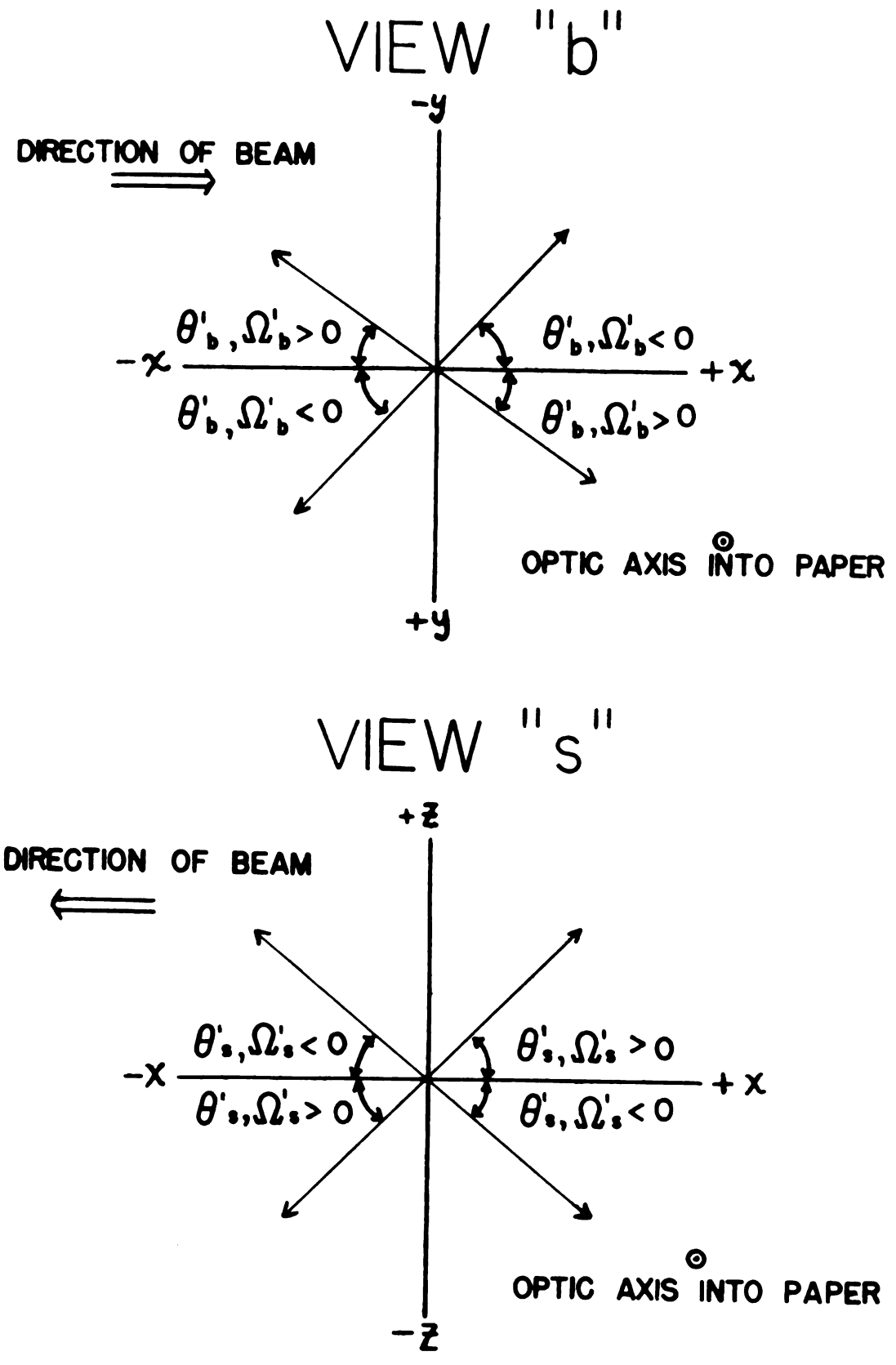
VIEW "b"
-y
DIRECTION OF BEAM
θ'b, Ω'b > 0
θ'b, Ω'b < 0
-x
+x
θ'b, Ω'b < 0
θ'b, Ω'b > 0
OPTIC AXIS ⊙ INTO PAPER
+y
VIEW "s"
+z
DIRECTION OF BEAM
θ's, Ω's < 0
θ's, Ω's > 0
-x
+x
θ's, Ω's > 0
θ's, Ω's < 0
OPTIC AXIS ⊙ INTO PAPER
-z

C. Coplanarity Test.

Inorder for an event to be classified as elastic, it must all lie in the same plane. Referring to figure 2A, the angle ϕ is the angle between the event plane and the chosen reference plane. If an event is to be classified as coplanor, each track composing the event must make the same angle ϕ with respect to the reference plane.

$$(22A) \quad \tan\phi = \frac{y_2^\circ - y_1^\circ}{z_2^\circ - z_1^\circ} = \frac{(y_2^\circ - y_1^\circ)/(x_2^\circ - x_1^\circ)}{(z_2^\circ - z_1^\circ)/(x_2^\circ - x_1^\circ)} = \frac{\tan\theta_b}{\tan\theta_s}$$

where the superscript $^\circ$ refers to the fact that these quantities are with respect to the beam track.

D. Sign Convention.

To satisfy our equations, we must restrict ourselves to certain sign conventions in the conically projected plane (screen). By referring to equation 5A and others, we see that the convention used in figure 3A is a suitable one.

E. Summary.

We have now all the equations necessary for solving θ and ϕ by measuring in the conical plane, Ω_b', θ_b', X_b, Y_b, Ω_s', θ'_s, X_s, Z_s. The eight equations are listed below.

$$(21A) \quad \tan\theta = (\tan^2\theta_b + \tan^2\theta_s)^{1/2}$$

$$(22A) \quad \tan\phi = \tan\theta_b / \tan\theta_s$$

(20A)
$$\tan\theta_b = (\tan\theta_b'' - \Omega_b') \div (1 + \Omega_b' \tan\theta_b'' + \Omega_s' \tan\theta_s'')$$
$$\tan\theta_s = (\tan\theta_s'' - \Omega_s') \div (1 + \Omega_b' \tan\theta_b'' + \Omega_s' \tan\theta_s'')$$

(18A)
$$\tan\theta_b'' = (\tan\theta_b' + B' \tan\theta_s') \div (1 - A'B')$$
$$\tan\theta_s'' = (\tan\theta_s' + A' \tan\theta_b') \div (1 - A'B')$$

(14A)
$$A' = (X_s \tan\theta_s' - Z_s) / k_s$$

(16A)
$$B' = (X_b \tan\theta_b' - Y_b) / k_b$$

The description of each of the quantities is listed in Table IA

view	symbol	description
"b" view	Ω_b'	angle beam makes with x axis
	θ_b'	angle particle makes with x axis
	X_b	co-ordinates of vertex
	Y_b	
"s" view	θ_s'	angle particle makes with x axis
	Ω_s'	angle beam makes with x axis
	X_s	co-ordinates of vertex
	Z_s	

Table IA.

A program for the calculation of θ and ϕ using the eight equations listed above has been set up for the computer Mistic located at Michigan State University.

BIBLIOGRAPHY

1. H. Yukawa, Proc. Phys.-Math. Soc. Japan, 17, 48 (1935).

2. R. G. Sachs, "Nuclear Theory," Addison Wesley 1953, p. 156-161.

3. H. A. Bethe & F. de Hoffmann, "Mesons," Row, Peterson, 1955, sect. 31d.

4. J. Ashkin, Phys. Rev. 96, 1104 (1954).

5. W. J. Willis, Ph.D. Thesis, Yale Univ. (1958).

6. Private Communication with Dr. Erwin.

7. D. Glaser & Rollig, "Proceedings of the 1958 Conference on High Energy Physics at CERN."

8. Private Communication from Dr. Ballam.

9. R. L. Cool, D. Clark, O. Piccioni, Phys. Rev. 103, 1082 (1956).

10. Private Communication with Dr. Cool.

11. R. Serber, Phys. Rev. 72, 1114 (1947).

12. J. Cladis, Thesis, Univ. of California, (1952).

13. Marshak, "Meson Physics," McGraw-Hill, 1952, p. 83-88.

14. We thank Dr. L. Leipuner for the results.

15. Marshak, loc. cit. p. 266.

16. B. Hahn, D. Ravenhall, & R. Hofstadter, Phys. Rev. 101, 1131 (1956).

17. The statistics in the problem does not warrant a more detailed treatment of the momentum.